NASA TECHNICAL MEMORANDUM

NASA TM X-3468

NASA TM X-3468

A GENERALIZED ORTHOGONAL COORDINATE SYSTEM FOR DESCRIBING FAMILIES OF AXISYMMETRIC AND TWO-DIMENSIONAL BODIES

Peter A. Gnoffo

Langley Research Center
Hampton, Va. 23665

NATIONAL AERONAUTICS AND SPACE ADMINISTRATION • WASHINGTON, D. C. • JUNE 1977

1. Report No.	2. Government Accession No.	3. Recipient's Catalog No.
NASA TM X-3468		

4. Title and Subtitle	5. Report Date
A GENERALIZED ORTHOGONAL COORDINATE SYSTEM FOR DESCRIBING FAMILIES OF AXISYMMETRIC AND TWO-DIMENSIONAL BODIES	June 1977
	6. Performing Organization Code

7. Author(s)	8. Performing Organization Report No.
Peter A. Gnoffo	L-11175
	10. Work Unit No.
	506-26-20-01

9. Performing Organization Name and Address	11. Contract or Grant No.
NASA Langley Research Center Hampton, VA 23665	
	13. Type of Report and Period Covered
12. Sponsoring Agency Name and Address	Technical Memorandum
National Aeronautics and Space Administration Washington, DC 20546	14. Sponsoring Agency Code

15. Supplementary Notes

16. Abstract

A generalized curvilinear orthogonal coordinate system is presented which can be used for approximating various axisymmetric and two-dimensional body shapes of interest to aerodynamicists. Such body shapes include spheres, ellipses, spherically capped cones, flat-faced cylinders with rounded corners, circular disks, and planetary probe vehicles. Also a set of transformation equations is developed whereby a uniform velocity field approaching a body at any angle of attack can be resolved in the transformed coordinate system. The Navier-Stokes equations are written in terms of a generalized orthogonal coordinate system to show the resultant complexity of the governing equations.

17. Key Words (Suggested by Author(s))	18. Distribution Statement
Generalized orthogonal coordinate systems Axisymmetric and two-dimensional bodies Navier-Stokes equations	Unclassified – Unlimited Subject Category 34

19. Security Classif. (of this report)	20. Security Classif. (of this page)	21. No. of Pages	22. Price*
Unclassified	Unclassified	59	$4.75

*For sale by the National Technical Information Service, Springfield, Virginia 22161

A GENERALIZED ORTHOGONAL COORDINATE SYSTEM FOR DESCRIBING FAMILIES OF AXISYMMETRIC AND TWO-DIMENSIONAL BODIES

Peter A. Gnoffo
Langley Research Center

SUMMARY

A generalized curvilinear orthogonal coordinate system is presented which can be used for approximating various axisymmetric and two-dimensional body shapes of interest to aerodynamicists. Such body shapes include spheres, ellipses, spherically capped cones, flat-faced cylinders with rounded corners, circular disks, and planetary probe vehicles. In addition, a set of transformation equations is developed whereby a uniform velocity field approaching a body at any angle of attack can be resolved in the transformed coordinate system. The expressions for the metric coefficients in this coordinate system are derived, and it is found that two of the metric coefficients are identically equal. The Navier-Stokes equations are written in terms of a generalized orthogonal coordinate system to show the resultant complexity of the governing equations. Also outlined is a solution procedure to obtain the flow field surrounding a planetary probe vehicle traveling at 0^{o} angle of attack at supersonic velocity through a perfect gas.

INTRODUCTION

The introduction of vector-processing computer systems has enhanced the feasibility of solving the full Navier-Stokes equations for compressible flow over various body shapes. However, the efficiency of vector processing is a function of how well (or how simply) a problem can be vectorized (ref. 1). In treating the flow over an axisymmetric body, it is advantageous if the body and the surrounding flow field can be transformed into a simple rectangular coordinate system. The vectorization is further simplified if the boundary conditions are transformed to one boundary of a rectangle, and the free-stream conditions are transformed to the opposite boundary of the rectangle.

In this paper an orthogonal coordinate system with these properties is presented for analytic body shapes which approximate spherically capped cones, flat-faced cylinders with rounded corners, circular disks, and planetary probe vehicles. The orthogonal coordinate system will also handle exactly the transformation of bodies with circular or elliptical cross sections.

SYMBOLS

A_n,B,C	constants of transformation
h	metric coefficient
H	total enthalpy
l_b	length of body
l_c	characteristic cone length defined in equation (14)
m	slope
N	integer
p	pressure
r	coordinate in transformed space
R	radius of curvature
s	arc length
t	time
T	temperature
u	velocity along line of constant r
v	velocity along line of constant θ
V	total velocity
x,y,z	coordinates in real space

Y_{max} maximum body radius

α angle of attack

γ ratio of specific heats

θ coordinate in transformed space

θ_{max} value of θ for maximum body radius

λ second coefficient of viscosity

μ viscosity

ρ density

τ_{ij} shear stress along surface perpendicular to i-axis in direction parallel to j-axis

ϕ coordinate in transformed space for axisymmetric case

ψ reference angle for line of constant r in real space

$\omega_1, \omega_2, \omega_3$ velocities in generalized coordinates

Subscripts:

b body

B base

c cone conditions

n nose

r	pertaining to conditions along line of constant θ and ϕ
s	shock
θ	pertaining to conditions along line of constant r and ϕ
ϕ	pertaining to conditions along line of constant r and θ
∞	free-stream conditions

DISCUSSION OF THE PROBLEM

The solution of the Navier-Stokes equations over a two-dimensional or axisymmetric body presents many difficulties in the computational formulation of the problem. One of the major factors which affects the complexity of the computational formulation is the choice of a suitable coordinate system to be used as a basis for differencing the governing equations.

There are basically two options available in the selection of such a coordinate system. The first option is simply to use either a rectangular coordinate system for a two-dimensional body or a cylindrical coordinate system for an axisymmetric body. The Navier-Stokes equations are in their simplest form (metric coefficients all equal to one) in a rectangular coordinate system so there is no need to calculate or store metric coefficients in a computer program. The Navier-Stokes equations written in a cylindrical coordinate system are only slightly more complicated and include a metric coefficient which varies as the distance from the axis of symmetry (ref. 2). However, there is no guarantee in either system that the body of the problem will pass through node points of the finite difference mesh used in the coordinate system (see fig. 1). Mesh points can be chosen to lie on the body surface, but the problem becomes more complex because a large amount of work is necessary in order to compute mesh points and boundary conditions for each different body shape which needs to be examined. This specification of mesh points will also force one to use differencing techniques based on unequal spacing at points close to the body. On the other hand, if mesh points are not made to lie on the body, some type of interpolation scheme has to be written into the program in order to compute boundary conditions and property derivatives on the body surface. Another problem with the rectangular and cylindrical coordinate systems is that there is no simple way of concentrating mesh points near the surface of an arbitrary body. Such a concentration is desirable because the viscous effects in a boundary layer lead to large gradients which will be inadequately defined by a coarse mesh.

In reference 3, Moretti describes a polar coordinate system (fig. 2) which is more realistic for describing two-dimensional and axisymmetric body shapes. This transformed coordinate system is generally nonorthogonal but does have the advantage of being able to map most arbitrary bodies onto a rectangle. Also mesh points can be concentrated near the body.

The second option available in the selection of a coordinate system is to choose a system based on the body itself. Within this option, two subgroups can be defined: an orthogonal body-oriented coordinate system and a natural coordinate system. Often an orthogonal body-oriented coordinate system can be used to describe bodies composed of combinations of spheres, cones, and other analytic body shapes. In this coordinate system, the coordinates of a point are determined by s (the distance along a body surface measured from the axis of symmetry) and n (the distance along a line which is normal to the body at s). A body-oriented coordinate system can be used, for example, to describe a spherically capped cone with a hemispherical afterbody joined smoothly at the corners (fig. 3(a)). The major problem with this system in this case is that four different sets of metric coefficients would have to be calculated, one set for each analytic section of the body. The body curvature, and consequently, one of the metric coefficients and the derivative with respect to s of another metric coefficient would not be continuous functions of s. The matching of flow properties at the boundaries of these various analytic sections and the formulation of the differencing procedure at these boundaries would add to the complexity of the problem. Also, in a body-oriented coordinate system, any discontinuity in slope on the body makes it impossible to describe a large section of the flow field. This situation would occur, for example, in attempting to describe the base flow for a sphere-cone configuration (fig. 3(b)). The body-oriented coordinate system would also break down when a concavity occurs in the body since the concavity leads to multiple specifications of some area in front of the concavity (see fig. 3(c)).

In a natural coordinate system, the body surface itself forms a boundary of a transformed computational space. Some obvious examples of this approach are a spherical coordinate system to describe flow over a sphere, a cylindrical coordinate system to describe flow over a cylinder, and a parabolic coordinate system to describe flow over a body with a parabolic cross section (fig. 4 and ref. 4). Metric coefficients for all of these coordinate systems are simple to calculate. Moreover, there is little difficulty in concentrating mesh points near the body because the computational mesh system is composed of lines parallel to the body which can be concentrated as close to the body as desired.

One very interesting natural coordinate system which is generally nonorthogonal is the "rock transformation" (ref. 5). Transformation functions are generated such that all boundaries of a problem are coincident with coordinate lines. The transformation of the governing equations results in a complex system of partial differential equations with

simple boundary conditions. Other interesting coordinate systems and coordinate transformations are outlined by Roache in reference 6.

In this paper, a more general natural orthogonal coordinate system is presented which can be used to approximate many different axisymmetric and two-dimensional body shapes. An example of this new coordinate system, shown in figure 5, transforms the area surrounding the body in real space into a rectangular computational grid. In this grid a finite length of one coordinate axis is the transformed body. As will be shown, the coordinate system is able to uniquely describe the area surrounding bodies with concavities. As might be expected, the expressions for the metric coefficients become more complicated; however, it turns out that two of the metrics are equal to each other. It can also be noted that for some of the bodies which can be described by this method a body-oriented coordinate system can be used to describe the area surrounding the analytic body. However, it is the development of the natural coordinate system that will be discussed in the following sections because that system can be used to describe the region surrounding all of the bodies presented in this paper.

GENERAL TRANSFORMATION

The transformation from the (θ,r,ϕ) domain to the (x,y,z) domain for an axisymmetric coordinate system is written as

$$\left.\begin{aligned} x(\theta,r,\phi) &= (-B \sinh r + C \cosh r) \cos\theta - \sum_{n=2}^{N} A_n e^{nr} \cos(n\theta) \\ y(\theta,r,\phi) &= \left[(B \cosh r - C \sinh r) \sin\theta + \sum_{n=2}^{N} A_n e^{nr} \sin(n\theta)\right] \cos\phi \\ z(\theta,r,\phi) &= \left[(B \cosh r - C \sinh r) \sin\theta + \sum_{n=2}^{N} A_n e^{nr} \sin(n\theta)\right] \sin\phi \end{aligned}\right\} \quad (1)$$

where N is a positive integer >2 and A_n, B, and C are arbitrary constants. A two-dimensional transformation to the xy-plane is obtained by setting $\phi = 0$.

Lines of constant r are perpendicular to lines of constant θ in the xy-plane. This relationship can be proved by showing that the slope m_θ of lines of constant r is equal to the negative inverse of the slope m_r of lines of constant θ where such lines intersect; that is,

$$m_\theta = \left.\frac{\partial y}{\partial x}\right)_r \approx \frac{\left.\frac{\partial y}{\partial \theta}\right)_r}{\left.\frac{\partial x}{\partial \theta}\right)_r} = \frac{(B \cosh r - C \sinh r)\cos\theta + \sum_{n=2}^{N} nA_n e^{nr}\cos(n\theta)}{(B \sinh r - C \cosh r)\sin\theta + \sum_{n=2}^{N} nA_n e^{nr}\sin(n\theta)} \tag{2}$$

$$m_r = \left.\frac{\partial y}{\partial x}\right)_\theta \approx \frac{\left.\frac{\partial y}{\partial r}\right)_\theta}{\left.\frac{\partial x}{\partial r}\right)_\theta} = \frac{(B \sinh r - C \cosh r)\sin\theta + \sum_{n=2}^{N} nA_n e^{nr}\sin(n\theta)}{(-B \cosh r + C \sinh r)\cos\theta - \sum_{n=2}^{N} nA_n e^{nr}\cos(n\theta)} \tag{3}$$

By inspection it is seen that $m_r = \frac{-1}{m_\theta}$.

Lines of constant r are transformed to circles in the xy-plane in the limit as r approaches negative infinity. This transformation can be verified by observing certain properties of the transformation. Terms involving the factor e^{nr} will vanish as r approaches negative infinity. Also note that -sinh r approaches cosh r as r approaches negative infinity. Therefore, for large negative r, equations (1) can be written approximately as

$$\left.\begin{aligned} x(\theta,r) &\approx \left[(B + C)\cosh r\right]\cos\theta \\ y(\theta,r) &\approx \left[(B + C)\cosh r\right]\sin\theta \end{aligned}\right\} \qquad (r << 0) \tag{4}$$

Equations (4), which are valid approximations to the transformation for large negative r, are the equation of a circle in the xy-plane with a radius equal to (B + C) cosh r. Also note that lines of constant θ become straight lines with slope m_r equal to $\tan\theta$ in the region where equations (4) are valid.

The line segment $r = 0,\ 0 \leqq \theta < 2\pi$ is transformed into a two-dimensional body in the xy-plane and becomes one boundary of the computational space in the θr-plane. An axisymmetric body is defined by mapping the line segment $r = 0,\ 0 \leqq \theta \leqq \pi$ to the xy-plane and rotating the image around the x-axis 2π rad. Thus,

Two dimensions

$$\left.\begin{aligned} x_b &= C\cos\theta - \sum_{n=2}^{N} A_n \cos(n\theta) \\ y_b &= B\sin\theta + \sum_{n=2}^{N} A_n \sin(n\theta) \end{aligned}\right\} \qquad (0 \leqq \theta < 2\pi) \qquad (5)$$

Axisymmetric

$$\left.\begin{aligned} x_b &= C\cos\theta - \sum_{n=2}^{N} A_n \cos(n\theta) \\ y_b &= \left[B\sin\theta + \sum_{n=2}^{N} A_n \sin(n\theta)\right]\cos\phi \\ z_b &= \left[B\sin\theta + \sum_{n=2}^{N} A_n \sin(n\theta)\right]\sin\phi \end{aligned}\right\} \qquad \begin{pmatrix} 0 \leqq \theta \leqq \pi \\ 0 \leqq \phi < 2\pi \end{pmatrix} \qquad (6)$$

The lines $\theta = 0$ and $\theta = 2\pi$ will therefore form two more boundaries of the computational space for a two-dimensional problem while the $\theta = 0$-plane, $\theta = \pi$-plane and the $\phi = 0$-plane, $\phi = 2\pi$-plane are the boundaries in computational space for an axisymmetric body. The final boundary of computational space is specified as $r = r_\infty$. The magnitude of r_∞ must be chosen large enough so that approximate boundary conditions can be applied.

It should be noted also that this transformation can be written as a conformal mapping for two dimensions. By setting $w = x(\theta,r) + iy(\theta,r)$, $E = (B + C)/2$, and $A_1 = (B - C)/2$ and by simplifying the result, one obtains

$$w = Ee^{iz} - \sum_{n=1}^{N} A_n e^{-inz}$$

where

$$z = \theta + ir$$

and

$$i = \sqrt{-1}$$

The problem which now remains is to pick the constants A_n, B, and C to describe the body of interest.

DETERMINATION OF BODY SHAPE

At first it appears that it might be possible to determine from equations (5) the constants A_n, B, and C for any body shape by using a Fourier transformation. However, once the constants for $y(\theta)$ have been specified, all but one of the constants for $x(\theta)$ are also specified. Therefore, it should not be expected that any arbitrary body shape can be produced by some systematic approach to determining the constants in equations (5). Also, once the body shape and the computational space are completely defined, the metric coefficients will have to be calculated. The calculation of these metrics (to be described later) becomes extremely tedious if N is large. Therefore, the approach taken in this section is to see the kind of body shapes that result by defining a small number of constants.

Families of Ellipses

For all $A_n = 0$ the transformation from the θr-plane to the xy-plane results in families of ellipses. For $B = C$ the transformation results in a circle of radius B (fig. 6(a)). For $B \neq C$ the transformation results in an ellipse (fig. 6(b)) of eccentricity e, where e is defined by the following equation (ref. 7):

$$e = \left(1 - \frac{B^2}{C^2}\right)^{1/2} \tag{7}$$

Families of Triangular Shapes

Families of triangular shapes occur when $A_2 \neq 0$ and $A_{n>2} = 0$. The radius of curvature on the body can be written as follows (ref. 7):

$$R = + \frac{\left[1 + \left(\frac{dy}{dx}\right)^2\right]^{3/2}}{\frac{d^2y}{dx^2}} = \left| \frac{\left[\left(\frac{\partial x}{\partial \theta}\right)^2 + \left(\frac{\partial y}{\partial \theta}\right)^2\right]^{3/2}}{\frac{\partial x}{\partial \theta}\frac{\partial^2 y}{\partial \theta^2} - \frac{\partial y}{\partial \theta}\frac{\partial^2 x}{\partial \theta^2}} \right| \tag{8}$$

The radius of curvature becomes infinite when the denominator of the last expression in equation (8) equals zero and the numerator is finite. For $B = C = 1$ and $A_2 = 1/4$, one can substitute into equation (8) to find that an infinite radius of curvature occurs for $\theta = 0$, $2\pi/3$, and $4\pi/3$ (fig. 7(a)). For $A_2 > 1/4$ or $A_2 < 1/4$ the body-shape change appears as is shown in figure 7. Care must be taken in that if A_2 is too large the body contour will intersect itself (fig. 7(c)). This condition is unacceptable for defining a real body shape in the xy-plane.

Also, in this three parameter system where A_2, B, and C are free parameters, there is the option of specifying three independent geometric conditions for a particular body type, and then it is possible to solve for A_2, B, and C. This approach was taken to define the bodies in figure 8 by specifying a nose radius of curvature R_n at $\theta = \pi$, an infinite radius of curvature at $\theta = 0$, and a maximum body radius Y_{max}.

Families of Rectangular Shapes

Families of rectangular shapes occur when $A_2 = 0$, $A_3 \neq 0$, and $A_{n>3} = 0$. If equations (5) are substituted into equation (8), then for $B = C = 1$ an infinite radius of curvature exists at $\theta = 0$, $\pi/2$, π, and $3\pi/2$ for $A_3 = 1/9$. The resulting body shape (fig. 9) approximates the cross section of a flat-faced cylinder with rounded corners. As with the triangular shapes, three independent geometric conditions can be specified in order to solve for A_3, B, and C. By specifying an infinite radius of curvature at $\theta = 0$, a total body length l_b, and a maximum body radius Y_{max}, the body shapes in figure 10 were constructed. Note that the body outlined in figure 10(b) can be used to approximate the cross section of a flat, circular disk.

Families of (N+1)-Sided Shapes

For $B = C = 1$ and $A_N = \frac{1}{N^2}$ with all other A_n equal to zero, a family of (N + 1)-sided shapes is produced. This can be shown as follows. Let

$$\left.\begin{aligned} x_b(\theta) &= \cos\theta - \frac{1}{N^2}\cos(N\theta) \\ y_b(\theta) &= \sin\theta + \frac{1}{N^2}\sin(N\theta) \end{aligned}\right\} \tag{9}$$

Substituting the above expression into equation (8) yields

$$R = \frac{\left\{\left[-\sin\theta + \frac{1}{N}\sin(N\theta)\right]^2 + \left[\cos\theta + \frac{1}{N}\cos(N\theta)\right]^2\right\}^{3/2}}{\left[-\sin\theta + \frac{1}{N}\sin(N\theta)\right]\left[-\sin\theta - \sin(N\theta)\right] - \left[\cos\theta + \frac{1}{N}\cos(N\theta)\right]\left[-\cos\theta + \cos(N\theta)\right]} \tag{10}$$

The denominator of equation (10) represented by D reduces to

$$D = \left(1 - \frac{1}{N}\right)\left\{1 - \cos\left[(N+1)\theta\right]\right\} \tag{11}$$

If $\theta = \frac{2k\pi}{N+1}$, then the denominator becomes

$$D = \left(1 - \frac{1}{N}\right)\left[1 - \cos(2k\pi)\right] = 0 \tag{12}$$

for k equal to 0 or an integer. Thus for $N = 3$ points of zero curvature (infinite radius of curvature) occur at $\theta = \frac{2k\pi}{4}$ for $k = 0, 1, 2,$ and 3. For $N = 4$ points of zero curvature are produced when $\theta = \frac{2k\pi}{5}$, and for $N = 5$ they are produced when $\theta = \frac{2k\pi}{6}$. Figures 11 and 12 show the resulting transformation into the xy-plane and demonstrate these conditions for $N = 4$ and $N = 5$.

Approximation to Spherically Capped Cones

A good approximation to spherically capped conical bodies can be obtained by including one extra parameter A_3 into the family of triangular shapes described in a previous section. Thus,

$$\left.\begin{aligned} x_b(\theta) &= C\cos\theta - A_3\cos(3\theta) - A_2\cos(2\theta) \\ y_b(\theta) &= B\sin\theta + A_3\sin(3\theta) + A_2\sin(2\theta) \end{aligned}\right\} \tag{13}$$

The constants A_2, A_3, B, and C are determined by simultaneously solving the equations specifying basic geometric parameters of a spherically capped cone, namely, θ_c, Y_{max}, and R_n (fig. 13). The base of the sphere cone at $\theta = 0$ is specified as

having zero curvature. The radius of curvature of the nose R_n at $\theta = \pi$ is specified. The value of θ_{max} for the maximum body radius is determined by setting $\frac{dy}{d\theta}(\theta_{max}) = 0$. The distance along the symmetry line l_c defined by the equation

$$l_c = x_b(\theta_{max}) - x_b(\pi) \tag{14}$$

is determined from the sphere-cone parameters by

$$l_c = \frac{Y_{max} \cos \theta_c - R_n(1 - \sin \theta_c)}{\sin \theta_c} \tag{15}$$

The maximum radius of the body Y_{max} is set equal to the base radius of the equivalent sphere cone. These equations can now be written as

$$C - 9A_3 - 4A_2 = 0 \tag{16}$$

$$\frac{(-B - 3A_3 + 2A_2)^2}{C - 9A_3 + 4A_2} = R_n \tag{17}$$

$$3A_3 \cos(3\theta_{max}) + 2A_2 \cos(2\theta_{max}) + B \cos \theta_{max} = 0 \tag{18}$$

$$-A_3 \cos(3\theta_{max}) - A_2 \cos(2\theta_{max}) + C \cos \theta_{max} - A_3 + A_2 + C = l_c \tag{19}$$

$$A_3 \sin(3\theta_{max}) + A_2 \sin(2\theta_{max}) + B \sin \theta_{max} = Y_{max} \tag{20}$$

Equations (16) to (20) can be solved numerically using Newton's method to obtain A_2, A_3, B, C, and θ_{max}. Specifications of various spherically capped cones and the equivalent transformed bodies appear in figures 14 to 18. True sphere cones are plotted over these bodies to demonstrate the agreement of the analytic approximation to the true body shape. For a ratio of nose radius to base radius equal to 1/2, fairly good agreement is obtained in the cone-angle range from 55^o to 60^o. The approximation becomes less accurate as the cone angle decreases. The forebodies of the analytic bodies for these low cone angles approximate hyperbolas better than sphere cones. A hyperbola of equivalent nose radius and asymptotic angle is plotted in figure 18. It is again cautioned that completely arbitrary specification must be avoided. For example, specifications for very wide angle bodies with small ratio of nose radius to base radius will result in bodies which loop

around and intersect themselves (fig. 19). Once a specific sphere-cone configuration is picked and the parameters A_3, A_2, B, and C are obtained, the transformed body should be plotted to determine whether or not agreement to the desired shape is satisfactory.

It should be noted that lines of constant r are concentrated near the body surface and lines of constant θ are concentrated in regions of sharp curvature. (See, for example, fig. 20.) This natural concentration of nodal points near the body surface should prove advantageous when solving the flow-field equations around the body using differencing techniques because the largest gradients in the flow-field variables typically occur near the body and at the corners of the body where severe expansion phenomena occur.

Planetary Probe Vehicles

A commonly considered configuration for planetary probe vehicles is a spherically capped conical forebody with a hemispherical afterbody. The forebody and the afterbody are blended together through a rounded curve at the shoulder as in figure 21. This configuration can be approximated by including one additional term A_4 to the sphere-cone approximation terms. Thus,

$$\left.\begin{aligned} x_b(\theta) &= -A_4 \cos(4\theta) - A_3 \cos(3\theta) - A_2 \cos(2\theta) + C \cos\theta \\ y_b(\theta) &= A_4 \sin(4\theta) + A_3 \sin(3\theta) + A_2 \sin(2\theta) + B \sin\theta \end{aligned}\right\} \tag{21}$$

As with the sphere-cone approximation, the constants in equations (21) can be determined by specifying the basic geometric parameters of a planetary probe vehicle. It is possible to solve for A_2, A_3, A_4, B, and C by defining a nose radius of curvature R_n, a base radius of curvature R_B, a vehicle length ℓ_b, a maximum body radius Y_{max}, and the length from the nose to the location of the maximum body radius on the symmetry line ℓ_c. To specify Y_{max} it is also necessary to determine θ_{max} such that $y(\theta_{max}) = Y_{max}$ and $\frac{dy}{d\theta}(\theta_{max}) = 0$. These specifications result in the following equations:

$$\frac{-(B + 4A_4 + 3A_3 + 2A_2)^2}{(-C + 16A_4 + 9A_3 + 4A_2)} = R_B \tag{22}$$

$$\frac{(-B + 4A_4 - 3A_3 + 2A_2)^2}{(C + 16A_4 - 9A_3 + 4A_2)} = R_n \tag{23}$$

$$2C - 2A_3 = l_b \tag{24}$$

$$A_4 \sin(4\theta_{max}) + A_3 \sin(3\theta_{max}) + A_2 \sin(2\theta_{max}) + B \sin \theta_{max} = Y_{max} \tag{25}$$

$$4A_4 \cos(4\theta_{max}) + 3A_3 \cos(3\theta_{max}) + 2A_2 \cos(2\theta_{max}) + B \cos \theta_{max} = 0 \tag{26}$$

$$-A_4 \cos(4\theta_{max}) - A_3 \cos(3\theta_{max}) - A_2 \cos(2\theta_{max}) + C \cos \theta_{max} + A_4 - A_3 + A_2 + C = l_c \tag{27}$$

Equations (22) to (27) can be solved using Newton's method to obtain A_4, A_3, A_2, B, C, and θ_{max}. Values for R_B, R_n, Y_{max}, l_b, and l_c were determined from figure 21 and then used to calculate the constants in equations (21). The approximating analytic body shape was then plotted and it appears in figure 22. Note that the afterbody in this figure is a better approximation to a blunt, spherically capped cone than to a hemisphere. This condition can be improved by specifying a much larger radius of curvature for the base than the true R_B of the actual vehicle. Also, the forebody cone angle and the nose radius-of-curvature specification for the analytic body were readjusted to agree more closely with the real body. The resulting analytic body shape (fig. 23) has an afterbody which looks like a hyperbola and which more closely approximates the shape of the real configuration as shown in figure 24.

METRIC COEFFICIENTS

The metric coefficients of an orthogonal curvilinear coordinate system are of the nature of scale factors which give the ratios of differential distances to the differentials of the coordinate parameters (ref. 8). The equations which are used to define the metric coefficients can be derived in the following manner. Consider the orthogonal transformation as defined in equations (1) for axisymmetric bodies. Let a θ-curve be defined in space as a line of constant r and constant ϕ in equations (1). If $\vec{r}$ is the position vector of a point P in space, then a tangent vector to the θ-curve is given by

$$\vec{\theta} = \frac{\partial \vec{r}}{\partial \theta} = \frac{\partial \vec{r}}{\partial s_\theta} \frac{ds_\theta}{d\theta} \tag{28}$$

where s_θ is the arc length along the θ-curve. The vector $\frac{\partial \vec{r}}{\partial s_\theta}$ is a unit vector tangent to the θ-curve which is redefined as $\vec{u}_\theta$ (see fig. 25). Equation (28) can now be rewritten as

$$\vec{\theta} = h_\theta \vec{u}_\theta \tag{29}$$

where $h_\theta = \dfrac{ds_\theta}{d\theta}$ is the length of $\vec{\theta}$. Therefore the relation for h_θ can be written as

$$h_\theta = \frac{ds_\theta}{d\theta} = \left|\frac{\partial \vec{r}}{\partial \theta}\right| = \left|\frac{\partial x}{\partial \theta}\,\vec{i} + \frac{\partial y}{\partial \theta}\,\vec{j} + \frac{\partial z}{\partial \theta}\,\vec{k}\right| \tag{30}$$

The geometric relationship between $\vec{\theta}$, $\vec{u}_\theta$, and h_θ on the θ-curve is shown in figure 25. The final expression for h_θ, along with h_r and h_ϕ which can be obtained in a similar manner, becomes

$$h_\theta^2 = \left(\frac{\partial x}{\partial \theta}\right)^2 + \left(\frac{\partial y}{\partial \theta}\right)^2 + \left(\frac{\partial z}{\partial \theta}\right)^2 = \left[(B \sinh r - C \cosh r) \sin\theta + \sum_{n=2}^{N} nA_n e^{nr} \sin(n\theta)\right]^2$$
$$+ \left[(B \cosh r - C \sinh r) \cos\theta + \sum_{n=2}^{N} nA_n e^{nr} \cos(n\theta)\right]^2 \tag{31}$$

$$h_r^2 = \left(\frac{\partial x}{\partial r}\right)^2 + \left(\frac{\partial y}{\partial r}\right)^2 + \left(\frac{\partial z}{\partial r}\right)^2 = \left[(-B \cosh r + C \sinh r) \cos\theta - \sum_{n=2}^{N} nA_n e^{nr} \cos(n\theta)\right]^2$$
$$+ \left[(B \sinh r - C \cosh r) \sin\theta + \sum_{n=2}^{N} nA_n e^{nr} \sin(n\theta)\right]^2 \tag{32}$$

$$h_\phi^2 = \left(\frac{\partial x}{\partial \phi}\right)^2 + \left(\frac{\partial y}{\partial \phi}\right)^2 + \left(\frac{\partial z}{\partial \phi}\right)^2 = \left[(B \cosh r - C \sinh r) \sin\theta + \sum_{n=2}^{N} A_n e^{nr} \sin(n\theta)\right]^2 \tag{33}$$

We note that $h_\theta^2 = h_r^2$ in equations (31) and (32). The metric coefficients are all positive in a right-handed coordinate system so long as $\vec{u}_\theta$ is in the same direction as $\vec{\theta}$, and $\vec{u}_r$ is in the same direction as $\vec{R}$. Therefore, it can be written that

$$\left.\begin{aligned} h_\theta &= h_r = h \\ h_\phi &= \left|y(\theta,r,0)\right| \end{aligned}\right\} \tag{34}$$

TRANSFORMATION OF UNIFORM VELOCITY FIELD

Note that in figure 20 the direction of increasing r is towards the body and the direction of increasing θ is counterclockwise around the body. The velocity component u is directed along lines of constant r in the direction of increasing θ. The velocity component v is directed along lines of constant θ in the direction of increasing r. Let a uniform velocity field of magnitude V_∞ approach a body in the xy-plane at angle of attack α. All angles are measured in standard trigonometric fashion from $\theta = 0$ in a counterclockwise direction. Let ψ be defined as the angle of the vector tangent to a line of constant r in the direction of increasing θ. In figure 26 it is clear that

$$\left.\begin{aligned} u &= V_\infty \cos(\psi - \alpha) = V_\infty(\cos\psi\cos\alpha + \sin\psi\sin\alpha) \\ v &= -V_\infty \sin(\psi - \alpha) = -V_\infty(\sin\psi\cos\alpha - \cos\psi\sin\alpha) \end{aligned}\right\} \tag{35}$$

It is now necessary to determine $\cos\psi$ and $\sin\psi$ as a function of r and θ.

The differentials dx and dy along a line of constant r can be determined from equations (1) in the xy-plane and are

$$\left.\begin{aligned} dx &= \left[(B\sinh r - C\cosh r)\sin\theta + \sum_{n=2}^{N} nA_n e^{nr}\sin(n\theta)\right]d\theta \\ dy &= \left[(B\cosh r - C\sinh r)\cos\theta + \sum_{n=2}^{N} nA_n e^{nr}\cos(n\theta)\right]d\theta \end{aligned}\right\} \tag{36}$$

From figure 27 and equations (32), (34), and (36), it can be shown that

$$\left.\begin{aligned}\cos\psi = \frac{dx}{\sqrt{dx^2 + dy^2}} &= \frac{\left[(B \sinh r - C \cosh r)\sin\theta + \sum_{n=2}^{N} nA_n e^{nr} \sin(n\theta)\right]}{h} \\ \sin\psi = \frac{dy}{\sqrt{dx^2 + dy^2}} &= \frac{\left[(B \cosh r - C \sinh r)\cos\theta + \sum_{n=2}^{N} nA_n e^{nr} \cos(n\theta)\right]}{h}\end{aligned}\right\} \quad (37)$$

TRANSFORMATION OF FLOW EQUATIONS AND BOUNDARY CONDITIONS

An example of the procedure used in applying the generalized orthogonal coordinate system can now be presented. Consider the problem of calculating the flow field surrounding the axisymmetric body described in figure 23 as this body moves through the atmosphere at hypersonic speed.

The body shape defined in figure 23 was generated with the following parameters substituted into equations (22) to (27):

$R_B = 3.55$ $\qquad$ $Y_{max} = 2.38$

$R_n = 1.10$ $\qquad$ $\theta_c = 53^o$

$l_b = 3.55$ $\qquad$ $l_c = l_c(\theta_c, R_n, Y_{max})$

Equations (22) to (27) were then solved using a Newton-Raphson iteration scheme to obtain

$A_4 = 0.068805390$

$A_3 = -0.071121784$

$A_2 = -0.047149036$

$B = 2.286877227$

$C = 1.703878216$

These constants completely specify the coordinate system which appears in figure 23, and are also substituted into equations (31) to (33) to obtain the metric coefficients.

In order to simplify the presentation here, it is assumed that the body is at 0° angle of attack to the incoming flow and that the fluid behaves as a perfect gas everywhere. Furthermore, it will be assumed that there is no radiative energy transfer nor any internal heat generation in the flow field.

By starting with the governing equations written for a general curvilinear orthogonal coordinate system (refs. 2 and 9), the following equations can be obtained:

Continuity

$$\frac{\partial}{\partial t}\left[h_1 h_2 h_3 \rho\right] + \frac{\partial}{\partial x_1}\left[h_2 h_3 \rho \omega_1\right] + \frac{\partial}{\partial x_2}\left[h_1 h_3 \rho \omega_2\right] = 0 \tag{38}$$

x_1-momentum

$$\begin{aligned}
&\frac{\partial}{\partial t}\left[h_1 h_2 h_3 \rho \omega_1\right] + \frac{\partial}{\partial x_1}\left[h_2 h_3 \left(p + \rho {\omega_1}^2 - \tau_{11}\right)\right] \\
&+ \frac{\partial}{\partial x_2}\left[h_1 h_3 \left(\rho \omega_1 \omega_2 - \tau_{21}\right)\right] - h_3 \left(p + \rho {\omega_2}^2 - \tau_{22}\right)\frac{\partial h_2}{\partial x_1} \\
&- h_2 \left(p - \tau_{33}\right)\frac{\partial h_3}{\partial x_1} + h_3 \left(\rho \omega_1 \omega_2 - \tau_{21}\right)\frac{\partial h_1}{\partial x_2} = 0
\end{aligned} \tag{39}$$

x_2-momentum

$$\begin{aligned}
&\frac{\partial}{\partial t}\left[h_1 h_2 h_3 \rho \omega_2\right] + \frac{\partial}{\partial x_1}\left[h_2 h_3 \left(\rho \omega_1 \omega_2 - \tau_{12}\right)\right] \\
&+ \frac{\partial}{\partial x_2}\left[h_1 h_3 \left(p + \rho {\omega_2}^2 - \tau_{22}\right)\right] - h_1 \left(p - \tau_{33}\right)\frac{\partial h_3}{\partial x_2} \\
&- h_3 \left(p + \rho {\omega_1}^2 - \tau_{11}\right)\frac{\partial h_1}{\partial x_2} + h_3 \left(\rho \omega_1 \omega_2 - \tau_{12}\right)\frac{\partial h_2}{\partial x_1} = 0
\end{aligned} \tag{40}$$

Energy

$$\frac{\partial}{\partial t}\left[h_1 h_2 h_3 \rho H\right] + \frac{\partial}{\partial x_1}\left[h_2 h_3 \left(\rho \omega_1 H - \omega_1 \tau_{11} - \omega_2 \tau_{21} + q_1\right)\right]$$

$$+ \frac{\partial}{\partial x_2}\left[h_1 h_3 \left(\rho \omega_2 H - \omega_1 \tau_{12} - \omega_2 \tau_{22} + q_2\right)\right] = 0 \tag{41}$$

Equation of state

$$p = \frac{\gamma - 1}{\gamma} \rho \left[H - \frac{1}{2}\left(\omega_1^{\,2} + \omega_2^{\,2}\right)\right] \tag{42}$$

where

$$\tau_{11} = 2\mu\left(\frac{1}{h_1}\frac{\partial \omega_1}{\partial x_1} + \frac{\omega_2}{h_1 h_2}\frac{\partial h_1}{\partial x_2}\right) + \frac{\lambda}{h_1 h_2 h_3}\left(\frac{\partial}{\partial x_1}\left(h_2 h_3 \omega_1\right) + \frac{\partial}{\partial x_2}\left(h_1 h_3 \omega_2\right)\right) \tag{43}$$

$$\tau_{22} = 2\mu\left(\frac{1}{h_2}\frac{\partial \omega_2}{\partial x_2} + \frac{\omega_1}{h_1 h_2}\frac{\partial h_2}{\partial x_1}\right) + \frac{\lambda}{h_1 h_2 h_3}\left(\frac{\partial}{\partial x_1}\left(h_2 h_3 \omega_1\right) + \frac{\partial}{\partial x_2}\left(h_1 h_3 \omega_2\right)\right) \tag{44}$$

$$\tau_{33} = 2\mu\left(\frac{\omega_1}{h_3 h_1}\frac{\partial h_3}{\partial x_1} + \frac{\omega_2}{h_2 h_3}\frac{\partial h_3}{\partial x_2}\right) + \frac{\lambda}{h_1 h_2 h_3}\left(\frac{\partial}{\partial x_1}\left(h_2 h_3 \omega_1\right) + \frac{\partial}{\partial x_2}\left(h_1 h_3 \omega_2\right)\right) \tag{45}$$

$$\tau_{12} = \tau_{21} = \mu\left(\frac{h_2}{h_1}\frac{\partial}{\partial x_1}\left(\frac{\omega_2}{h_2}\right) + \frac{h_1}{h_2}\frac{\partial}{\partial x_2}\left(\frac{\omega_1}{h_1}\right)\right) \tag{46}$$

$$q_i = -\frac{\mu}{p_r h_i}\frac{\partial}{\partial x_i}\left[H - \frac{1}{2}\left(\omega_1^{\,2} + \omega_2^{\,2}\right)\right] \tag{47}$$

In equations (38) to (47), the x_1 coordinate is defined as θ and the x_2 coordinate as r.

The metric coefficients can now be calculated from equations (31) to (33) and substituted into the governing differential equations with

$$h_1 = h_\theta = h \tag{48}$$

$$h_2 = h_r = h \tag{49}$$

$$h_3 = h_\phi \tag{50}$$

$$\frac{\partial}{\partial x_1} = \frac{\partial}{\partial \theta} \tag{51}$$

$$\frac{\partial}{\partial x_2} = \frac{\partial}{\partial r} \tag{52}$$

$$w_1 = u \tag{53}$$

$$w_2 = v \tag{54}$$

(Derivatives with respect to ϕ are equal to 0 since this is an axisymmetric flow.)

In figure 23 the stagnation streamline for 0^o angle of attack coincides with the lines of constant θ for $\theta = 0$ and $\theta = \pi$. For $\theta = 0$ or $\theta = \pi$, it can be seen from equations (31) to (33) that $h_\phi = 0$, $\frac{\partial h_\phi}{\partial r} = 0$, and $\frac{\partial h}{\partial \theta} = 0$ on the stagnation line. The limiting form of the governing equations on the stagnation streamline can now be obtained by differentiating equations (38) to (41) with respect to θ. Thus, for $\theta = 0$ or $\theta = \pi$,

Continuity

$$\frac{\partial}{\partial t}\left[h^2\rho\right] + 2\frac{\partial}{\partial \theta}\left[h\rho u\right] + \frac{\partial}{\partial r}\left[h\rho v\right] + h\rho v \frac{\frac{\partial^2 h_\phi}{\partial r\, \partial \theta}}{\frac{\partial h_\phi}{\partial \theta}} = 0 \tag{55}$$

θ-momentum

$$u = 0 \tag{56}$$

r-momentum

$$\frac{\partial}{\partial t}\left[h^2 \rho v\right] + 2\frac{\partial}{\partial \theta}\left[h\left(\rho uv - \tau_{12}\right)\right] + \frac{\partial}{\partial r}\left[h\left(p + \rho v^2 - \tau_{22}\right)\right]$$

$$- \frac{\partial h}{\partial r}\left(p - \tau_{11}\right) + \frac{\dfrac{\partial^2 h_\phi}{\partial \theta\, \partial r}}{\dfrac{\partial h_\phi}{\partial \theta}} h\left(\rho v^2 + \tau_{33} - \tau_{22}\right) = 0 \tag{57}$$

Energy

$$\frac{\partial}{\partial t}\left[h^2 \rho H\right] + 2\frac{\partial}{\partial \theta}\left[h\left(\rho uH - u\tau_{11} - v\tau_{21} + q_1\right)\right]$$

$$+ \frac{\partial}{\partial r}\left[h\left(\rho vH - v\tau_{22} + q_2\right)\right]$$

$$+ h\left(\rho vH - v\tau_{22} + q_2\right)\frac{\dfrac{\partial^2 h_\phi}{\partial r\, \partial \theta}}{\dfrac{\partial h_\phi}{\partial \theta}} = 0 \tag{58}$$

where on the stagnation line

$$\tau_{12} = \tau_{21} = 0 \tag{59}$$

$$\tau_{11} = 2\mu\left(\frac{1}{h}\frac{\partial u}{\partial \theta} + \frac{v}{h^2}\frac{\partial h}{\partial r}\right) + \frac{\lambda}{h^2}\left(\frac{\partial}{\partial \theta}(hu) + h\frac{\partial u}{\partial \theta} + \frac{\partial}{\partial r}(hv) + hv\frac{\dfrac{\partial^2 h_\phi}{\partial \theta\, \partial r}}{\dfrac{\partial h_\phi}{\partial \theta}}\right) \tag{60}$$

$$\tau_{22} = 2\mu\left(\frac{1}{h}\frac{\partial v}{\partial r}\right) + \frac{\lambda}{h^2}\left(\frac{\partial}{\partial\theta}(hu) + h\frac{\partial u}{\partial\theta} + \frac{\partial}{\partial r}(hv) + hv\frac{\dfrac{\partial^2 h_\phi}{\partial\theta\,\partial r}}{\dfrac{\partial h_\phi}{\partial\theta}}\right) \tag{61}$$

$$\tau_{33} = 2\mu\left(\frac{1}{h}\frac{\partial u}{\partial\theta} + \frac{v}{h}\frac{\dfrac{\partial^2 h_\phi}{\partial\theta\,\partial r}}{\dfrac{\partial h_\phi}{\partial\theta}}\right) + \frac{\lambda}{h^2}\left(\frac{\partial}{\partial\theta}(hu) + h\frac{\partial u}{\partial\theta} + \frac{\partial}{\partial r}(hv) + hv\frac{\dfrac{\partial^2 h_\phi}{\partial\theta\,\partial r}}{\dfrac{\partial h_\phi}{\partial\theta}}\right) \tag{62}$$

The boundary conditions on the body are

No slip

$$u(\theta) = 0$$

$$v(\theta) = 0$$

Adiabatic wall

$$\frac{\partial T}{\partial r}(\theta) = 0$$

The boundary conditions at $\theta = 0$ (the afterbody stagnation line) and $\theta = \pi$ (the forebody stagnation line) are

$$u(r) = 0$$

$$\frac{\partial v}{\partial\theta}(r) = 0$$

$$\frac{\partial p}{\partial\theta}(r) = 0$$

$$\frac{\partial \rho}{\partial\theta}(r) = 0$$

$$\frac{\partial H}{\partial\theta}(r) = 0$$

Outflow boundary conditions must be applied at $r = r_\infty$. The manner in which the boundary conditions can be specified or approximated is a question which must be examined. However, it should be noted that due to the exponential stretching of the mesh as the magnitude of r increases, nominal values of r_∞ can move the outflow boundary far away from the body. For example, if some approximate outflow boundary conditions can be calculated at a distance of 100 body lengths downstream, then r_∞ can be calculated for this problem using equations (4) as $r_\infty = -5.181$.

It is also possible to map the outflow boundary to infinity and retain orthogonality by using an additional coordinate transformation. For example, the coordinate transformation

$$r = a \ln \eta$$

will map

$$-\infty < r \leqq 0 \quad \text{to} \quad 0 < \eta \leqq 1$$

where a is an arbitrary constant.

An explicit time-dependent scheme with appropriate initial conditions can now be used to program the governing equations in the rectangular domain of figure 23. (The details of any particular solution technique and the computational problems associated with it are not the subject of this paper.) The equations can then be integrated forward in time until a steady state is reached and a final flow-field solution is obtained.

CONCLUDING REMARKS

A transformation procedure has been presented which has the capability of making analytic approximations to axisymmetric and two-dimensional body shapes of interest to aerodynamicists. The transformation from a rectangular domain in the θr-plane results in an orthogonal coordinate system in the xy-plane which surrounds the specified body shape. Configurations which can be modeled by this procedure include spheres, axisymmetric ellipses, spherically capped cones, flat-faced cylinders with rounded corners, circular disks, and planetary probe-vehicle shapes. Good approximations to spherically capped cones are obtained for bodies having a ratio of nose radius to base radius of 1/2 and cone angles varying from 55° to 60°.

This transformation procedure should be well adapted to vector-processing computer systems because the body boundary conditions can be easily calculated along one

boundary of a computational plane. Also there is no need to divide the computational plane into a forebody flow region and an afterbody flow region.

Langley Research Center
National Aeronautics and Space Administration
Hampton, VA 23665
February 16, 1977

REFERENCES

1. Weilmuenster, K. James; and Howser, Lona M.: Solution of a Large Hydrodynamic Problem Using the STAR 100 Computer. NASA TM X-73904, 1976.

2. Hughes, William F.; and Gaylord, Eber W.: Basic Equations of Engineering Science. Schaum Pub. Co., c.1964.

3. Moretti, Gino; and Salas, Manuel D.: The Blunt Body Problem for a Viscous Rarefied Gas Flow. AIAA Paper No. 69-139, Jan. 1969.

4. Peyret, Roger; and Viviand, Henri: Calculation of the Flow of a Viscous Compressible Fluid Around an Obstacle of Parabolic Shape. NASA TT F-16558, 1975.

5. Thompson, Joe F.; Thames, Frank C.; and Mastin, C. Wayne: Automatic Numerical Generation of Body-Fitted Curvilinear Coordinate System for Field Containing Any Number of Arbitrary Two-Dimensional Bodies. J. Comput. Phys., vol. 15, no. 3, July 1974, pp. 299-319.

6. Roache, Patrick J.: Computational Fluid Dynamics. Hermosa Publ., c.1972.

7. Baumeister, Theodore, ed.: Marks' Mechanical Engineers' Handbook. Sixth ed. McGraw-Hill Book Co., Inc., 1958.

8. Hildebrand, Francis B.: Advanced Calculus for Applications. Prentice-Hall, Inc., 1962.

9. Back, L. H.: Conservation Equations of a Viscous, Heat-Conducting Fluid in Curvilinear Orthogonal Coordinates. Tech. Rep. 32-1332 (Contract No. NAS 7-100), Jet Propul. Lab., California Inst. Technol., Sept. 15, 1968.

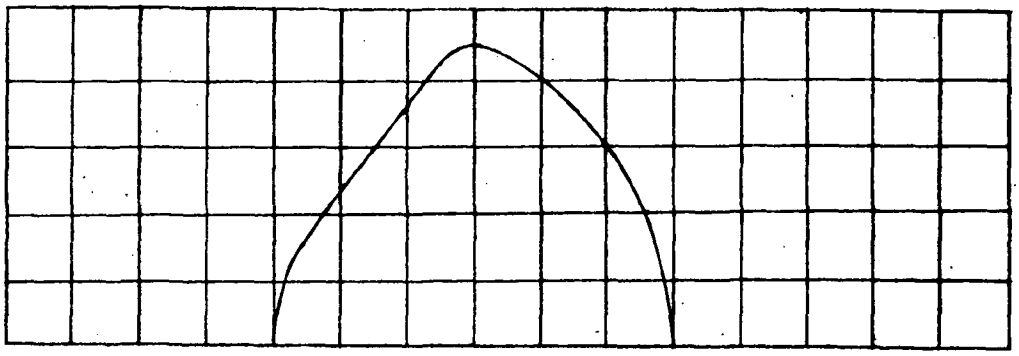

Figure 1.- Rectangular coordinate system over two-dimensional body.

$$y = \pi - \theta$$

$$x = \frac{r - r_b(\theta)}{r_s(\theta) - r_b(\theta)}$$

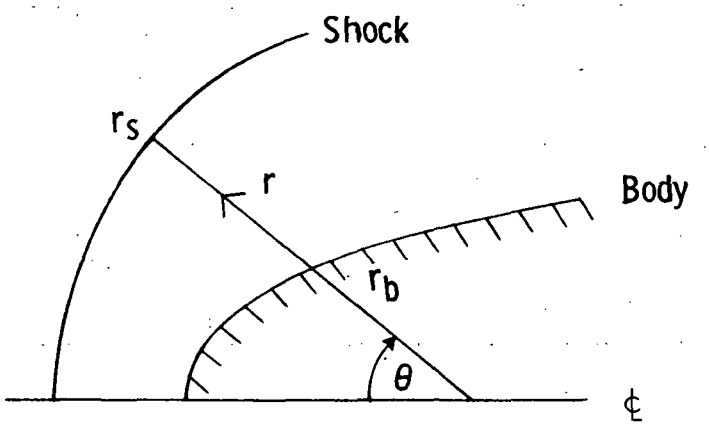

Figure 2.- Polar transformation for blunt-body calculations.

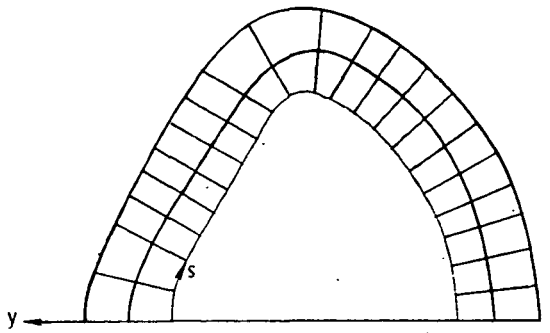

(a) Spherically capped cone with hemisphere afterbody.

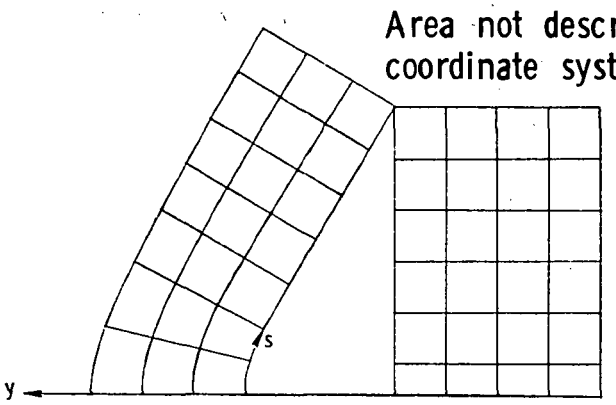

(b) Spherically capped cone.

Coordinates of A = (s_1, y_1) (s_2, y_1) (s_3, y_1)

Coordinates of B = (s_4, y_3) (s_1, y_2)

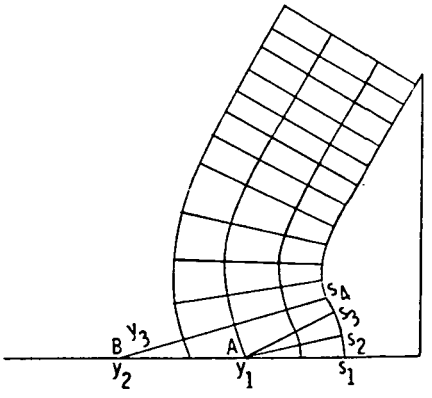

(c) Body with concavity.

Figure 3.- Body-oriented coordinate system.

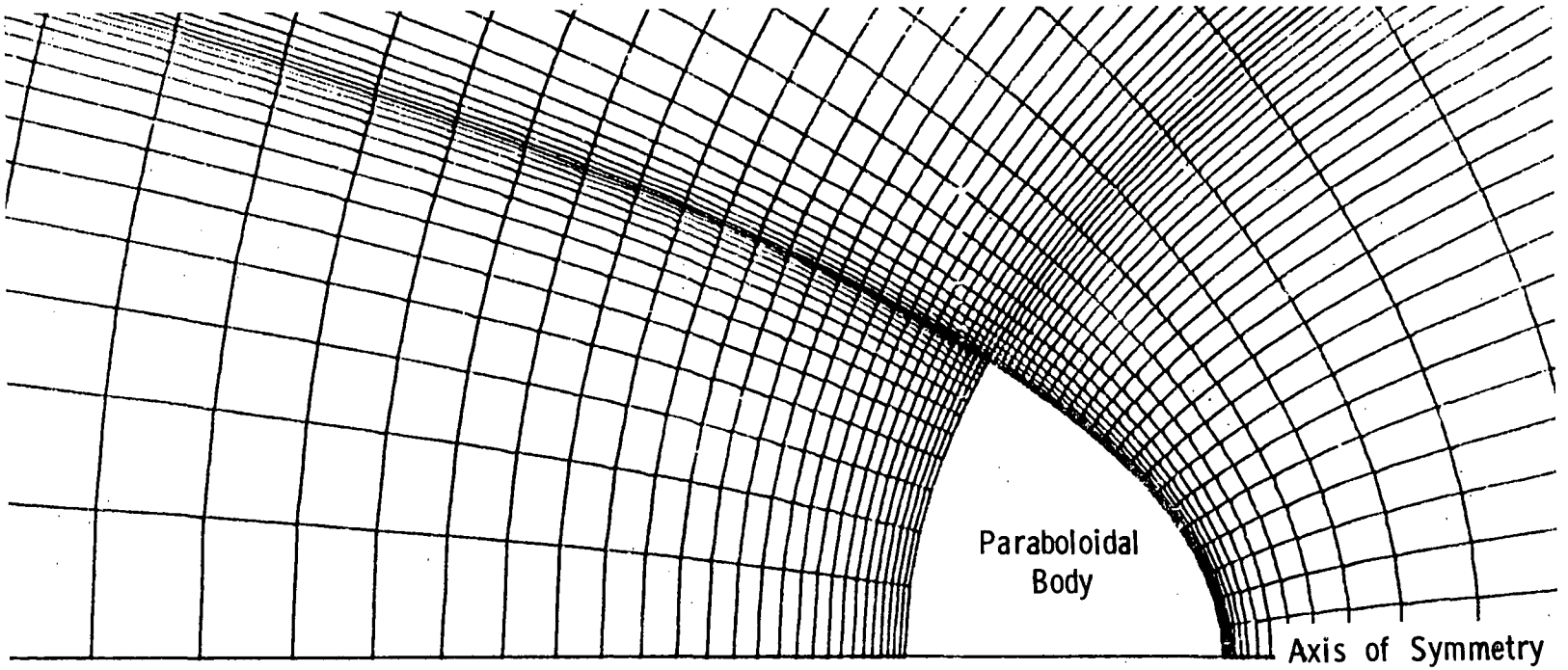

Figure 4.- Parabolic natural coordinate system.

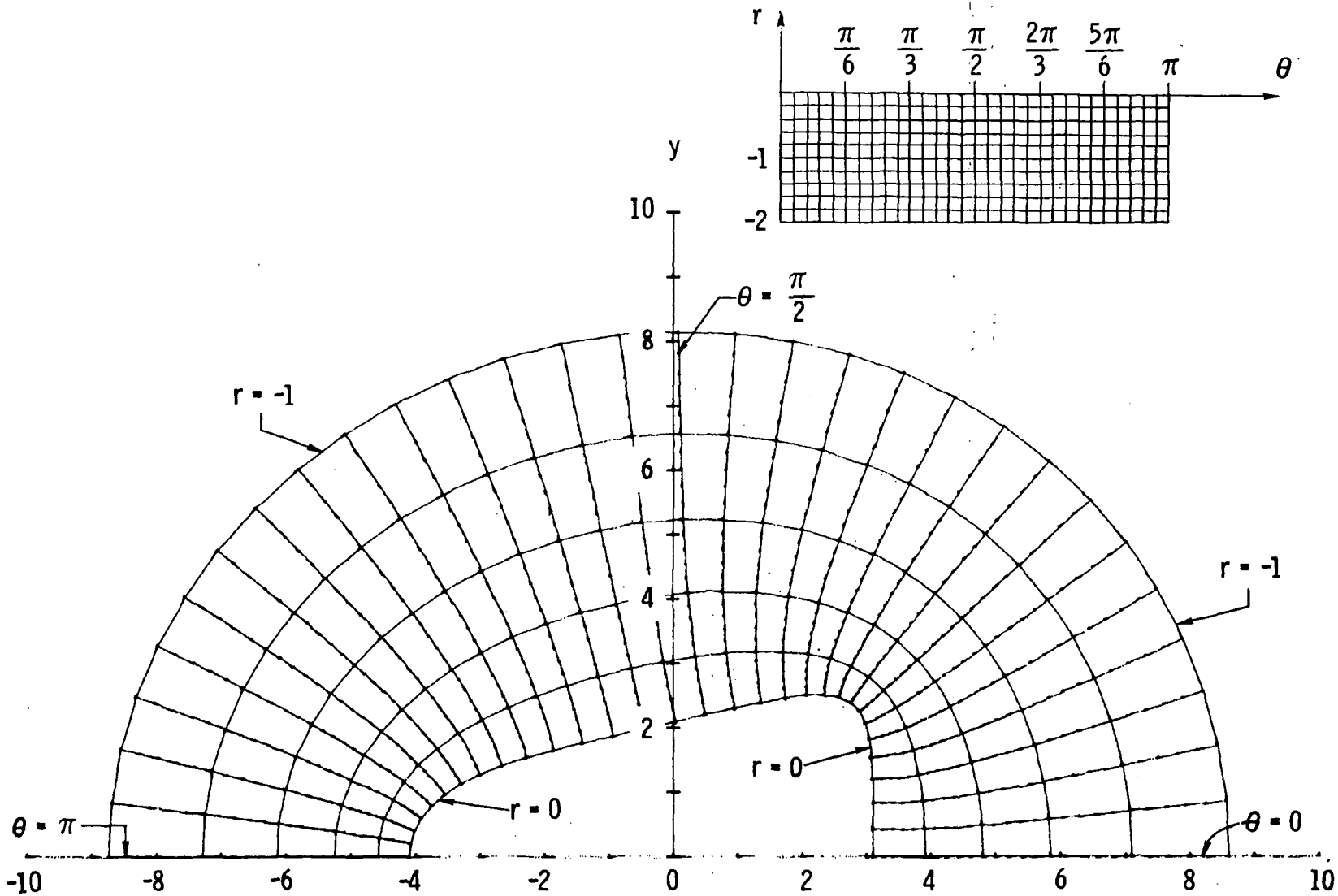

Figure 5.- Generalized natural orthogonal coordinate system.

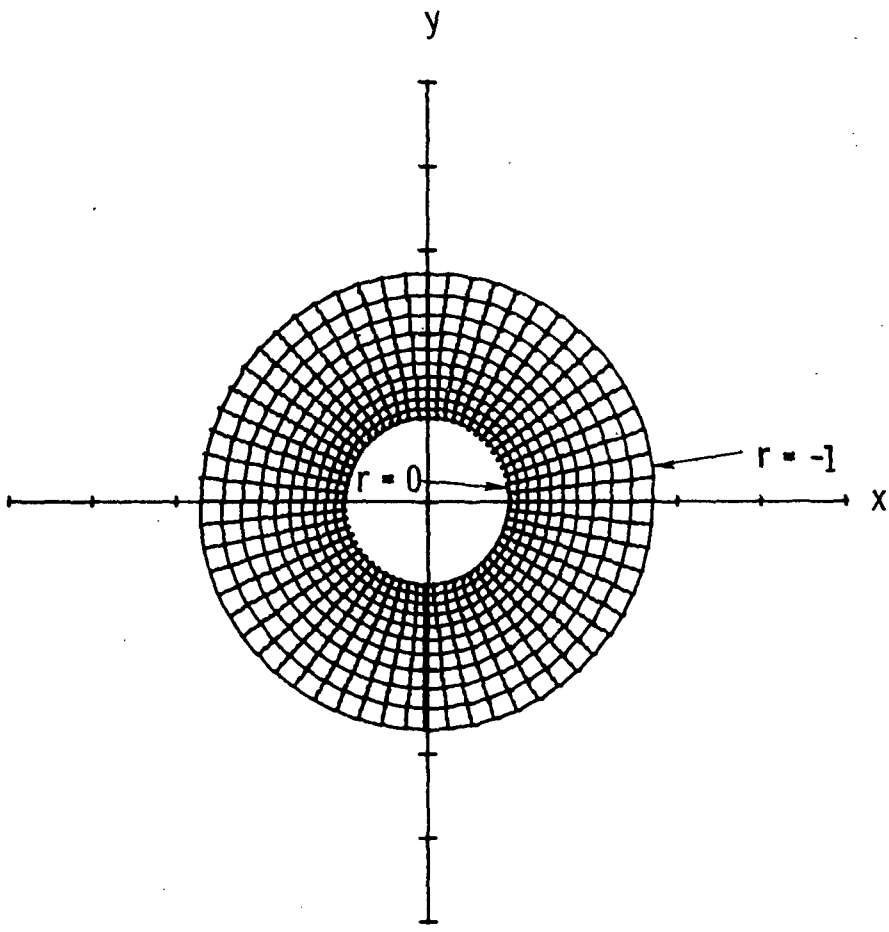

(a) C = 1.

Figure 6.- Family of ellipses for B = 1.

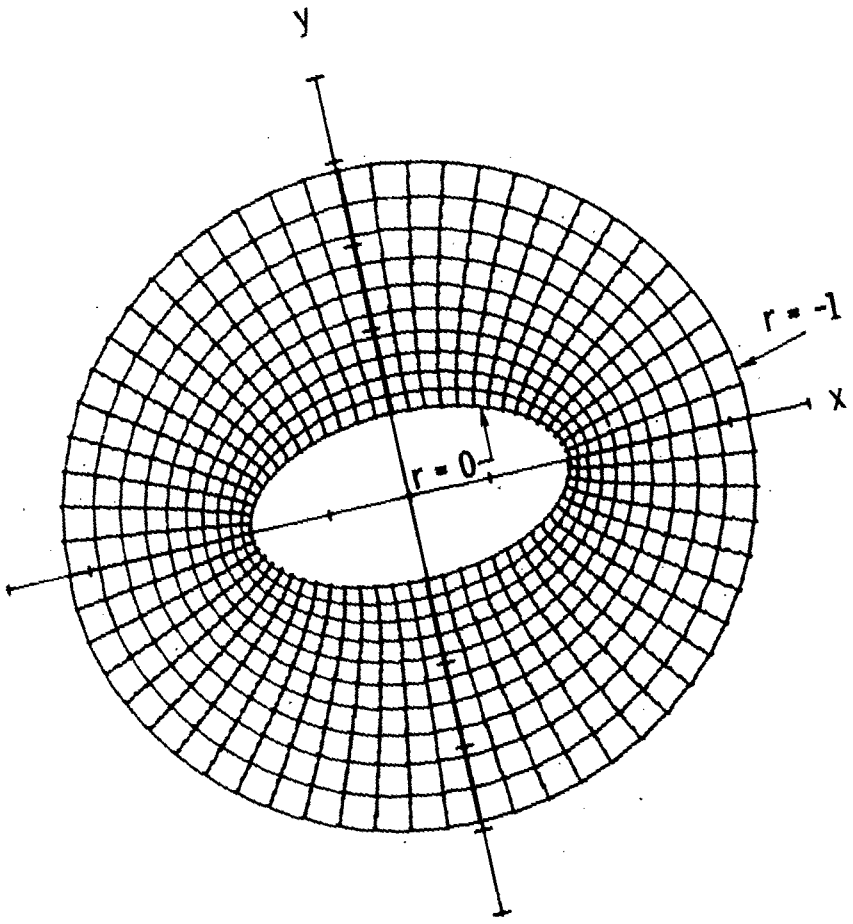

(b) C = 2.

Figure 6.- Concluded.

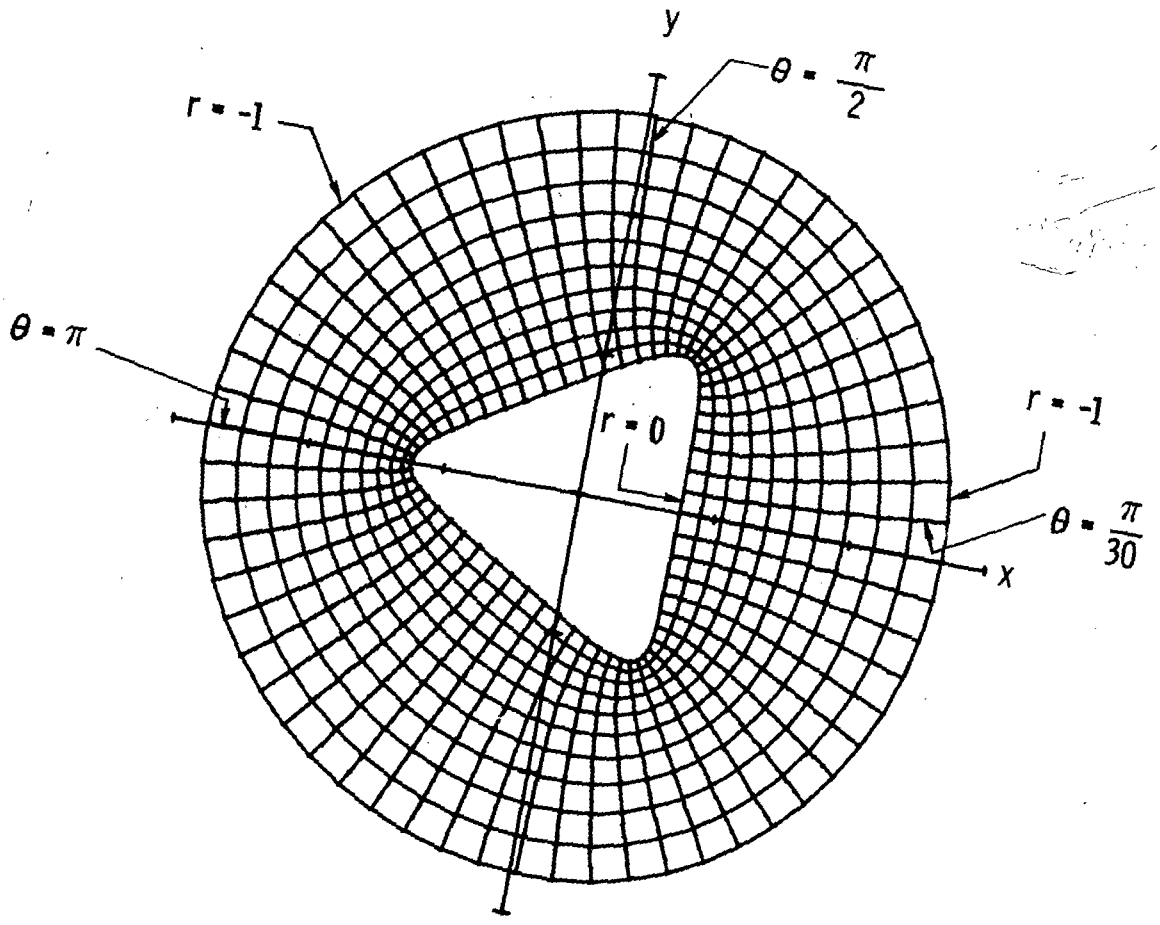

(a) $A_2 = 0.25$.

Figure 7.- Family of triangular shapes for $B = 1$ and $C = 1$.

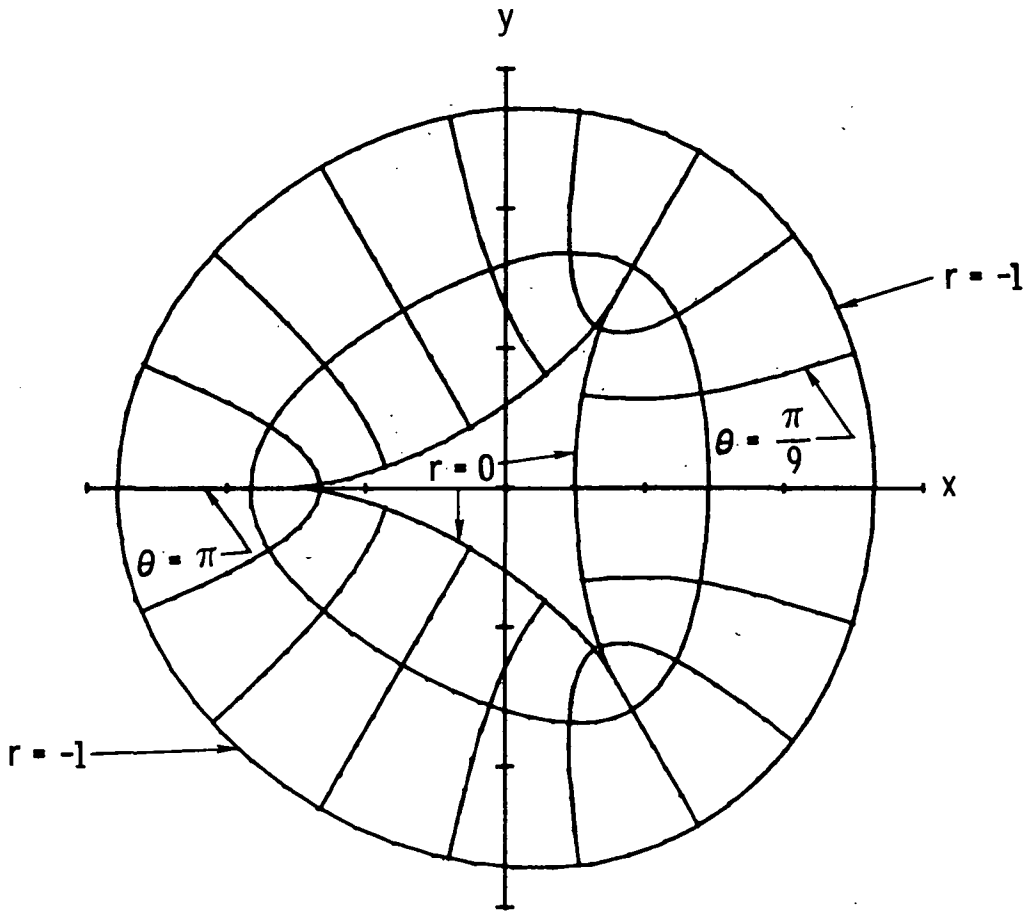

(b) $A_2 = 0.5$.

Figure 7.- Continued.

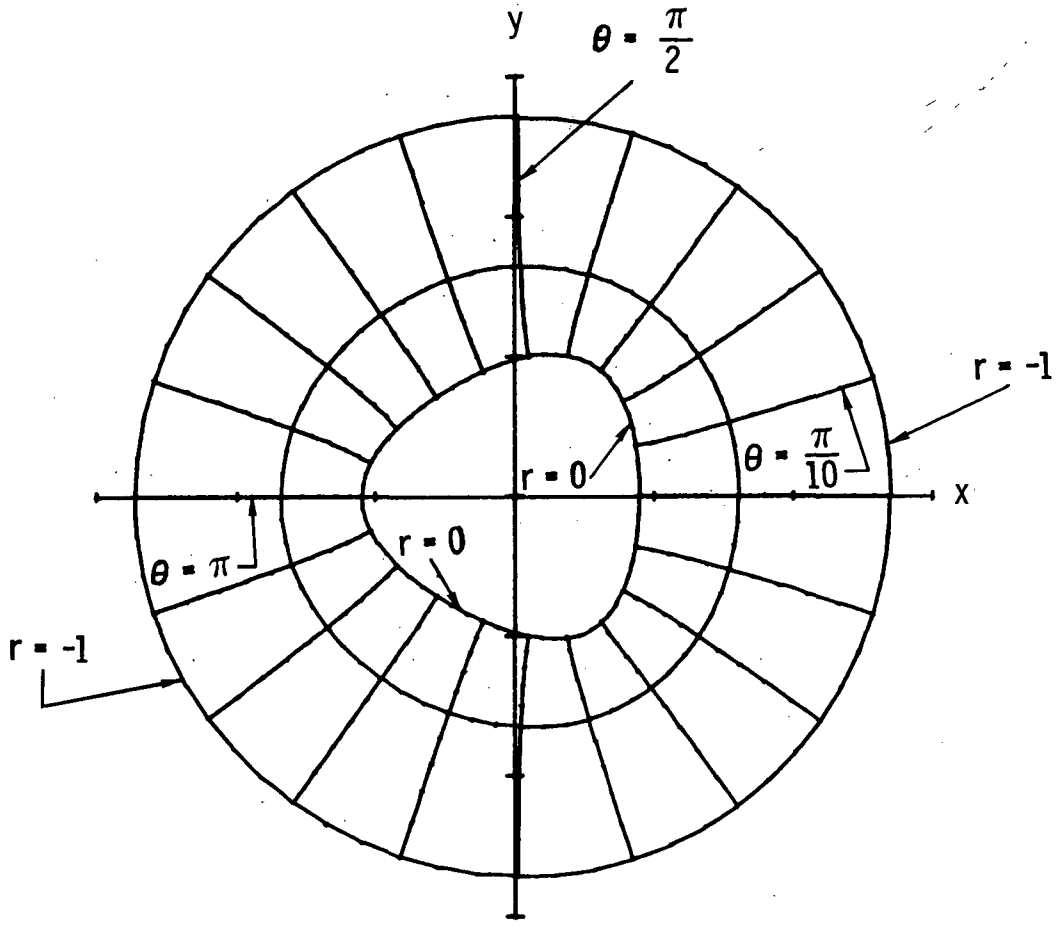

(c) $A_2 = 0.1$.

Figure 7.- Continued.

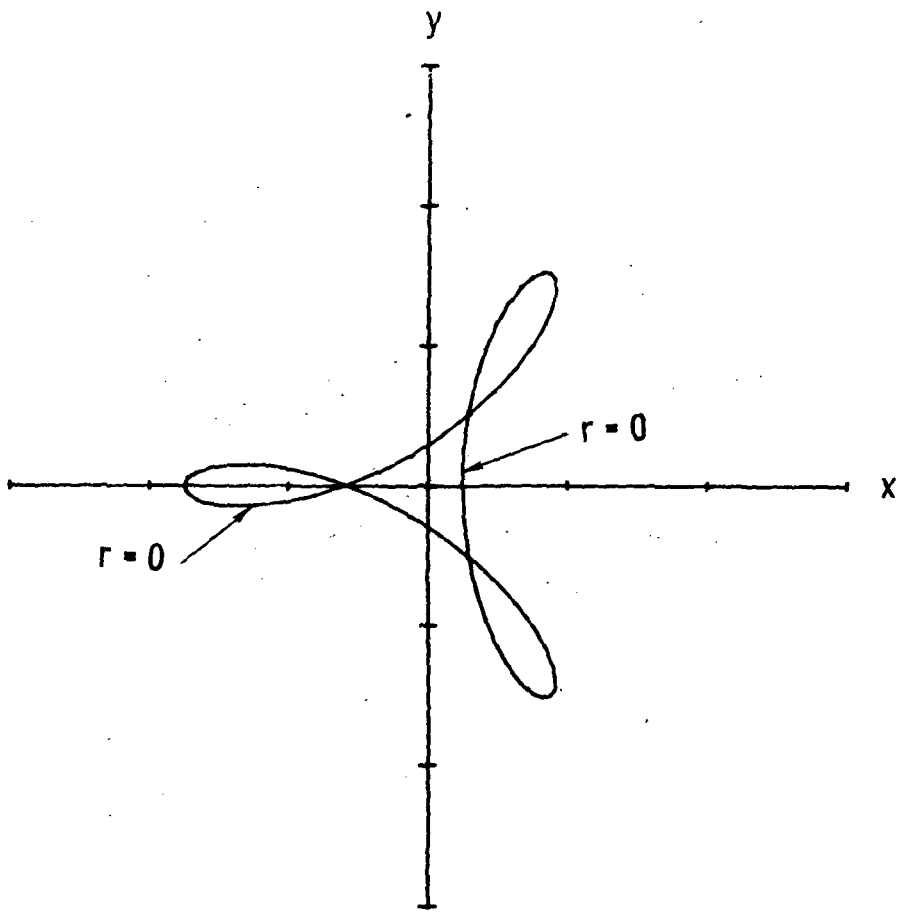

(d) $A_2 = 0.75$.

Figure 7.- Concluded.

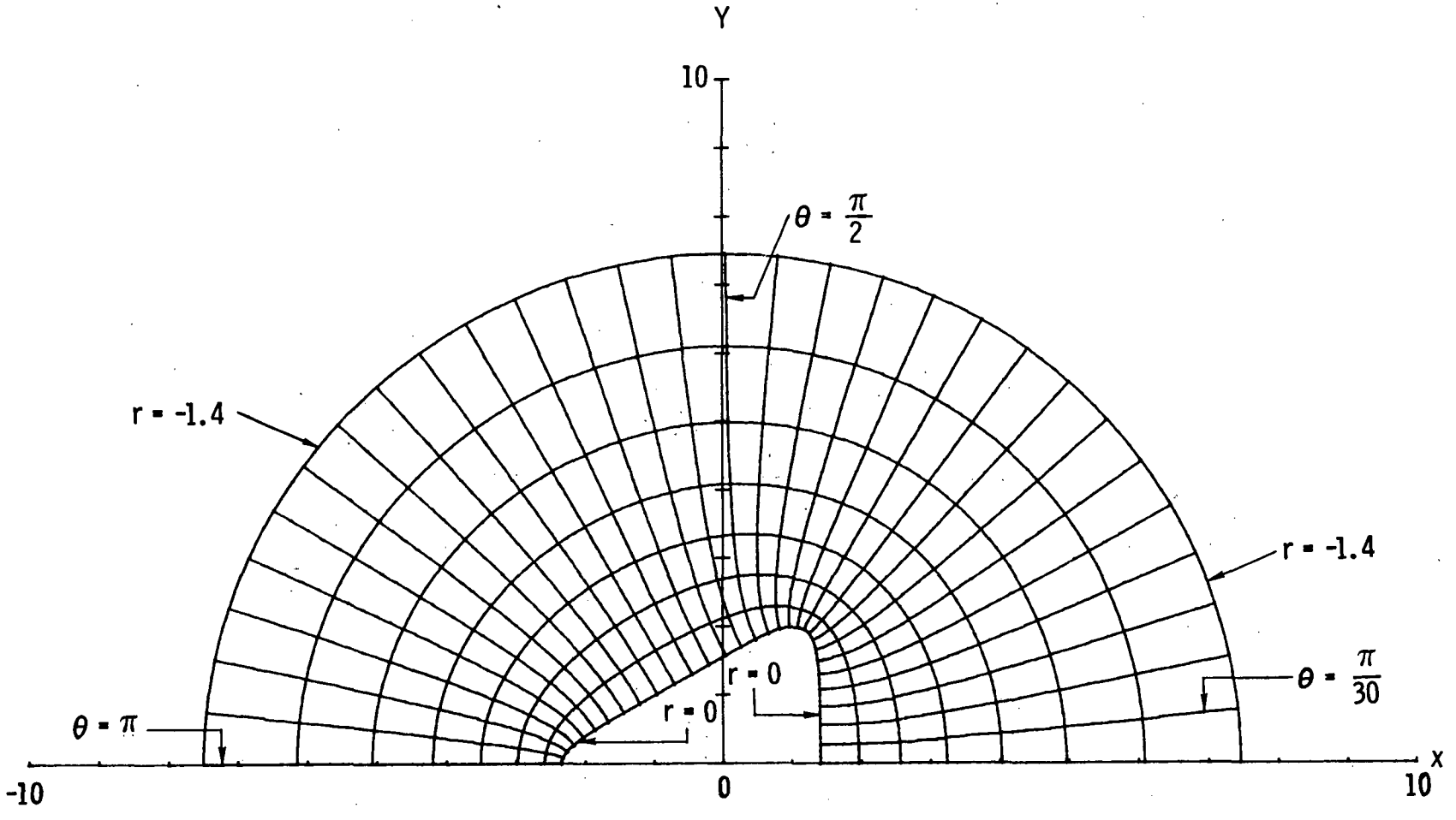

(a) $R_n = 0.2$.

Figure 8.- Family of triangular shapes for $Y_{max} = 2$.

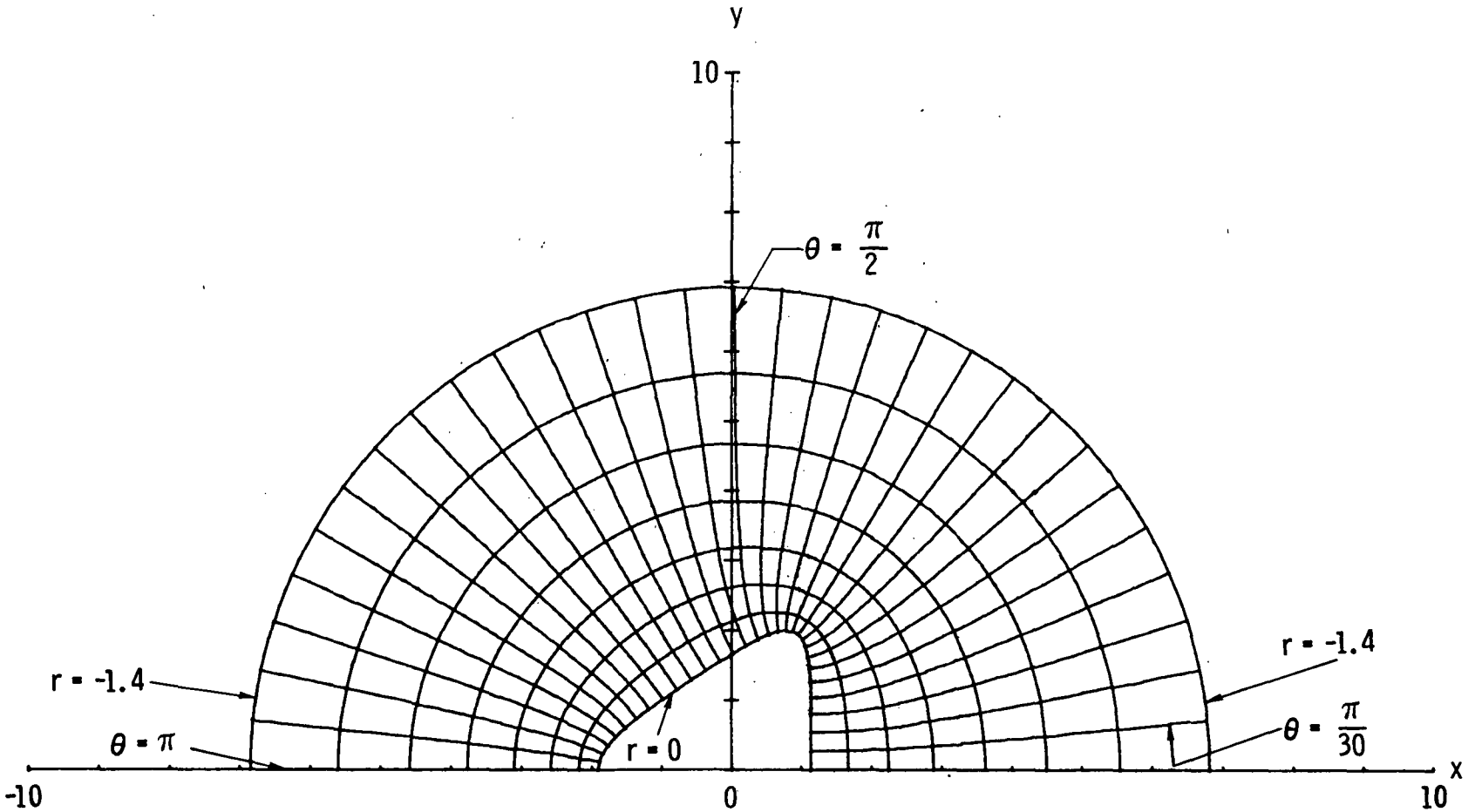

(b) $R_n = 0.4$.

Figure 8.- Continued.

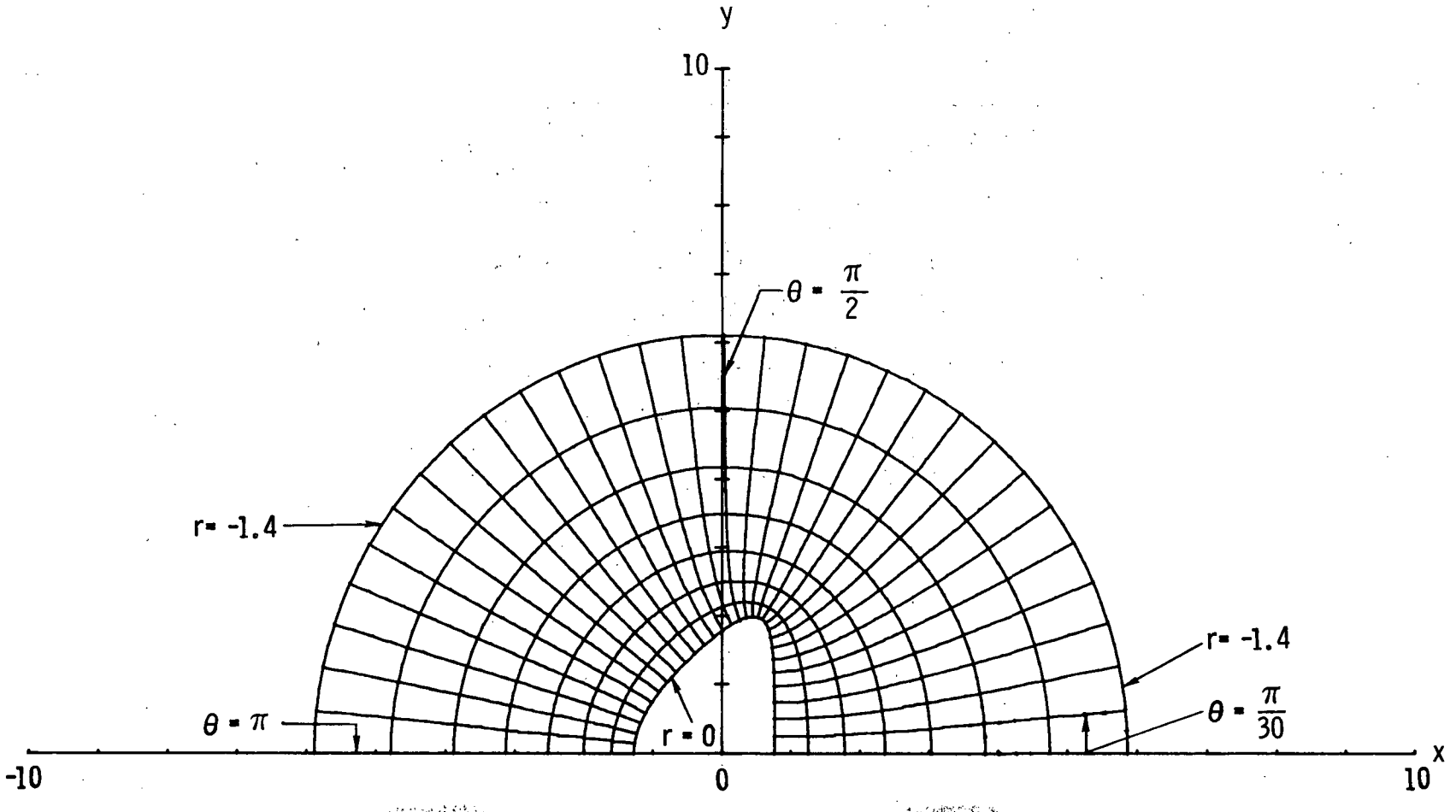

(c) $R_n = 1.0$.

Figure 8.- Continued.

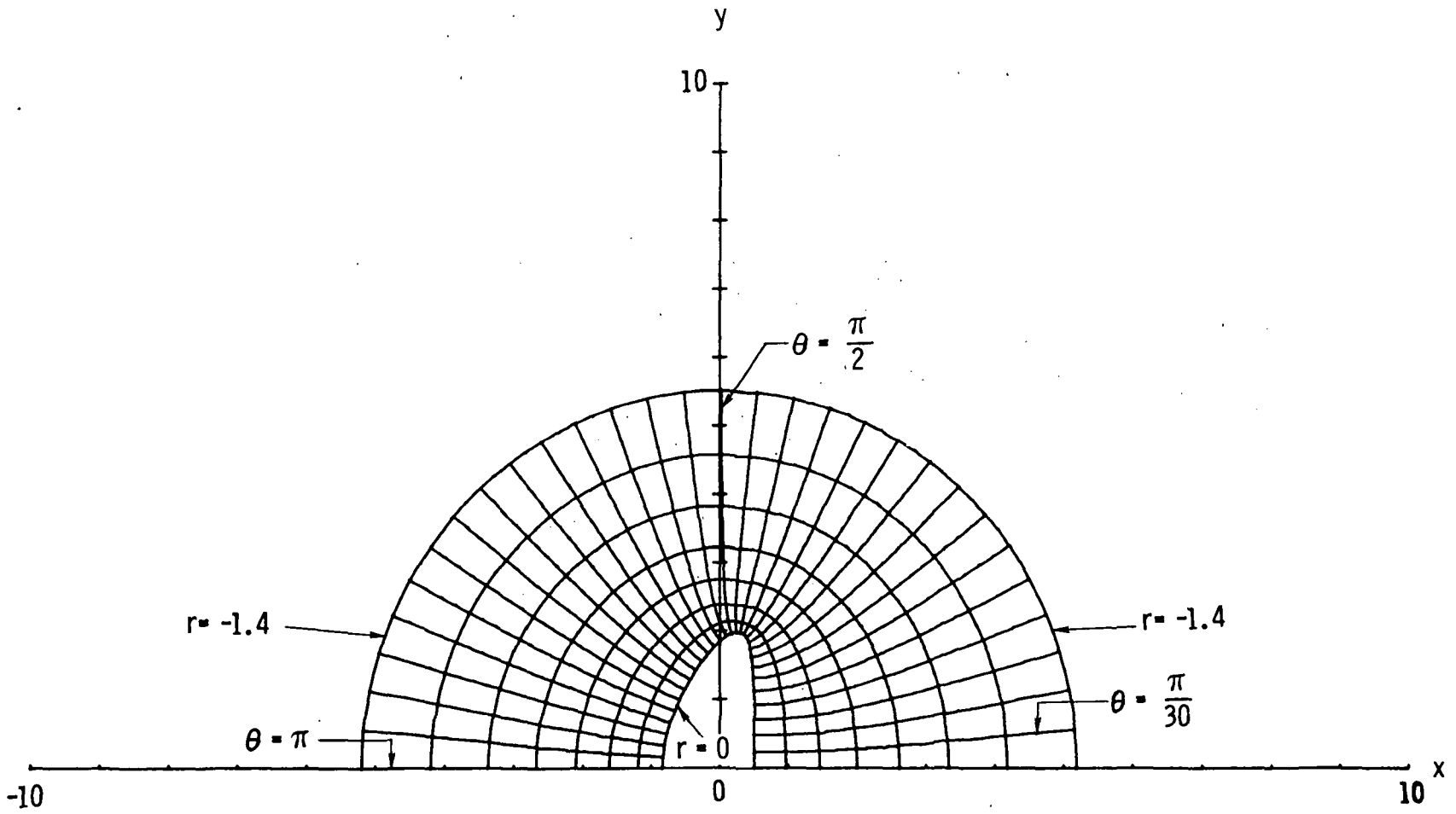

(d) $R_n = 2.0$.

Figure 8.- Concluded.

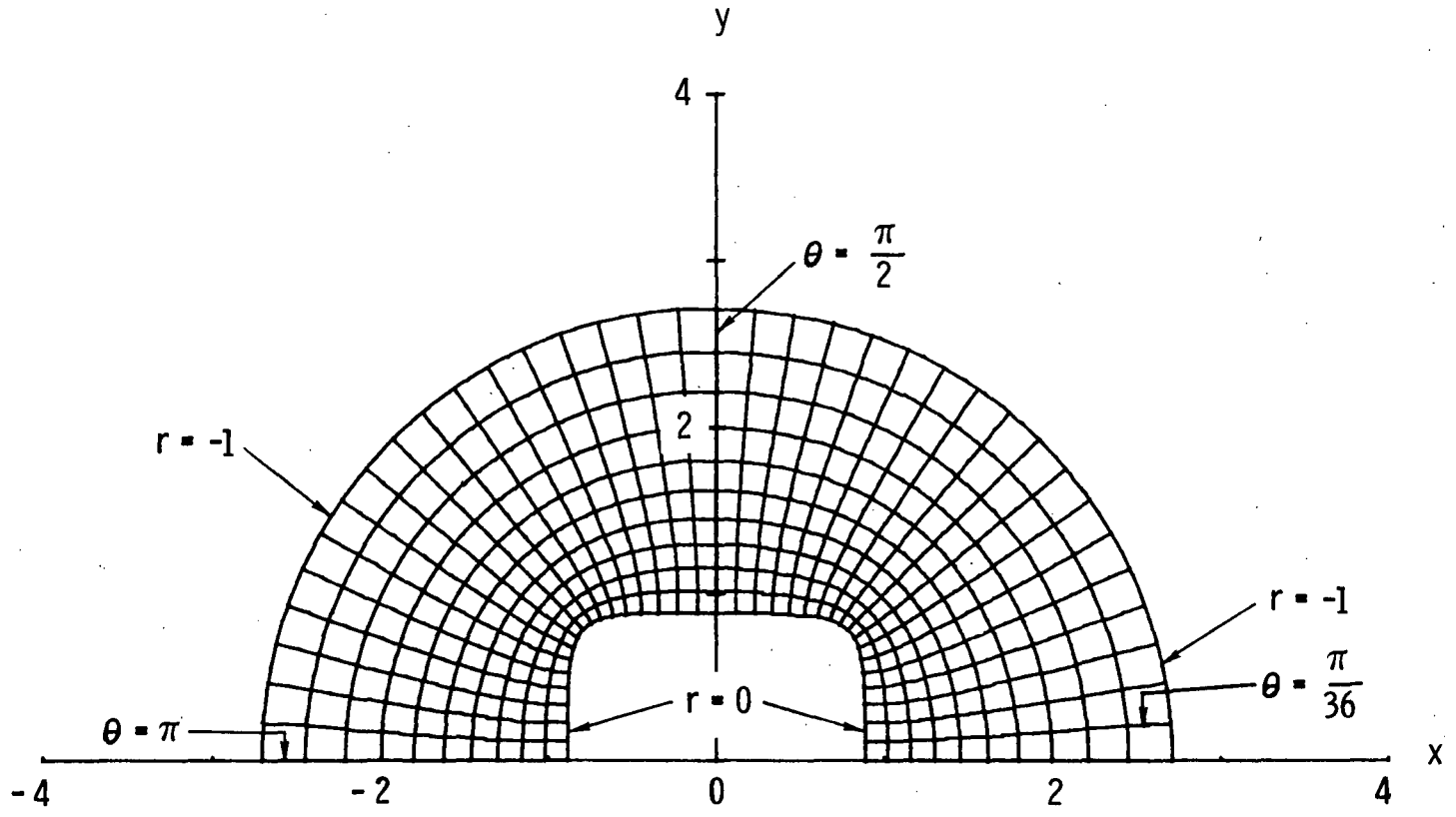

Figure 9.- Family of rectangular shapes for $A_3 = 1/9$, $B = 1$, and $C = 1$.

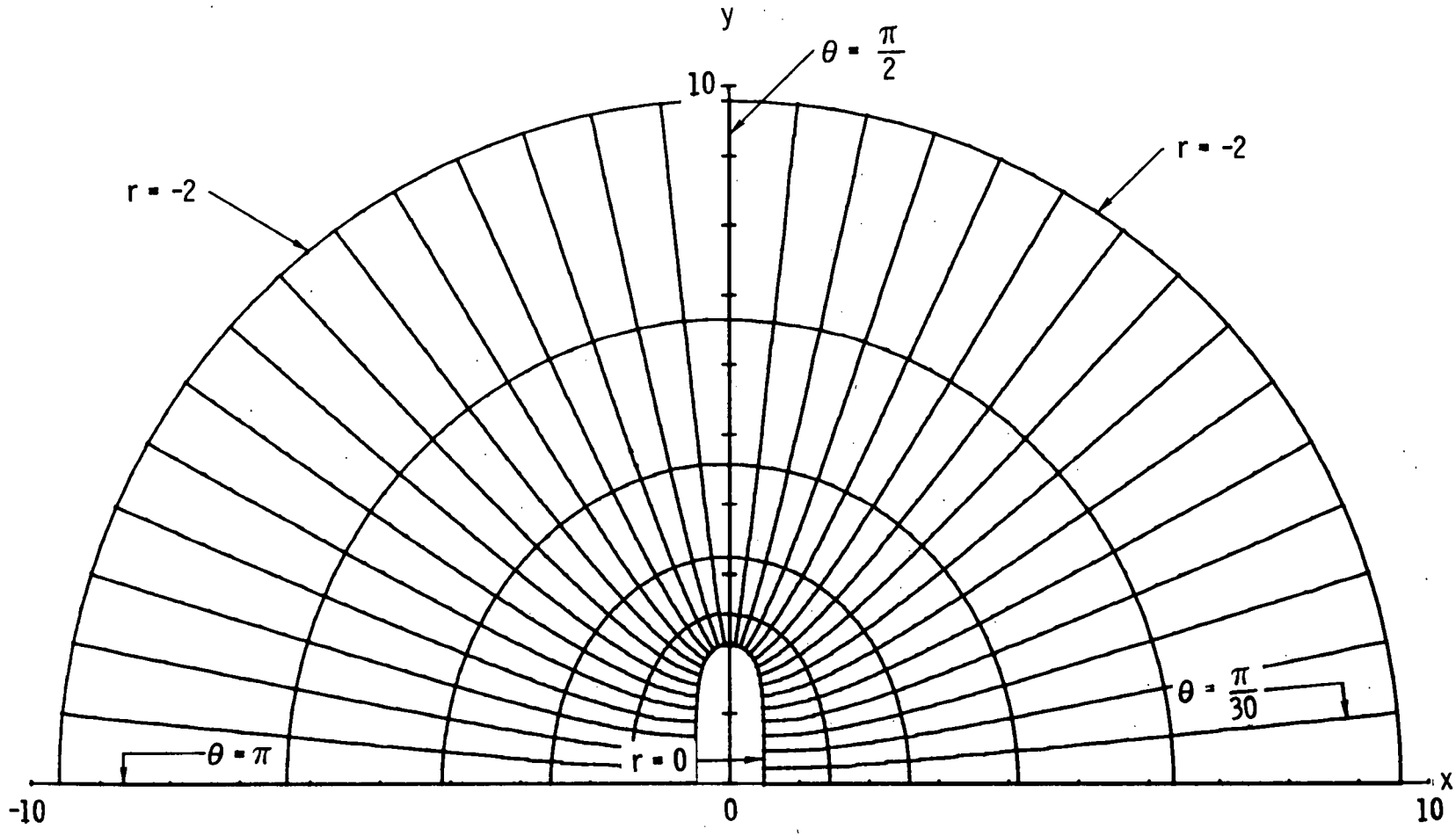

(a) L = 1.0.

Figure 10.- Family of rectangular shapes for $Y_{max} = 2$.

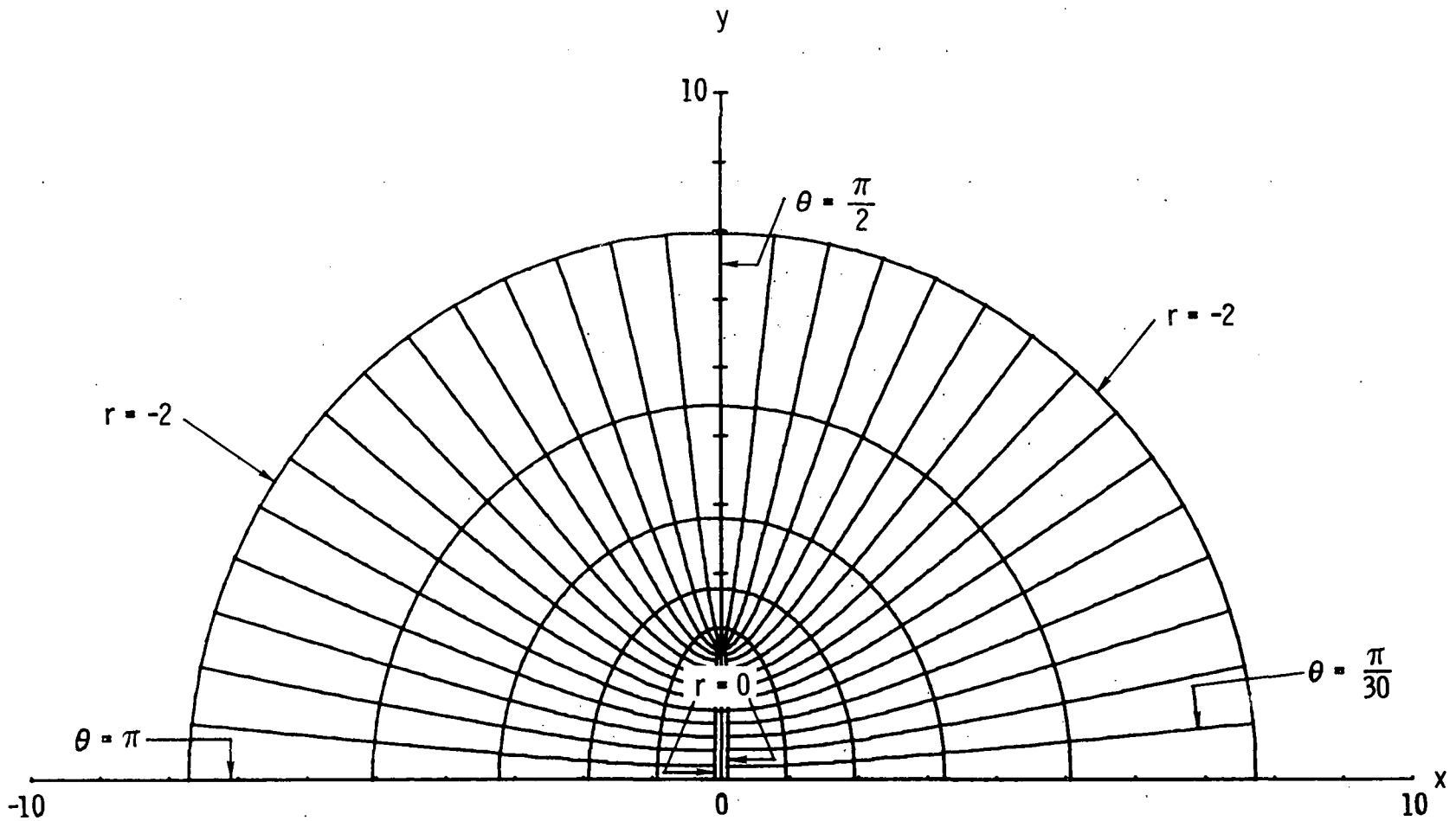

(b) L = 0.2.

Figure 10.- Concluded.

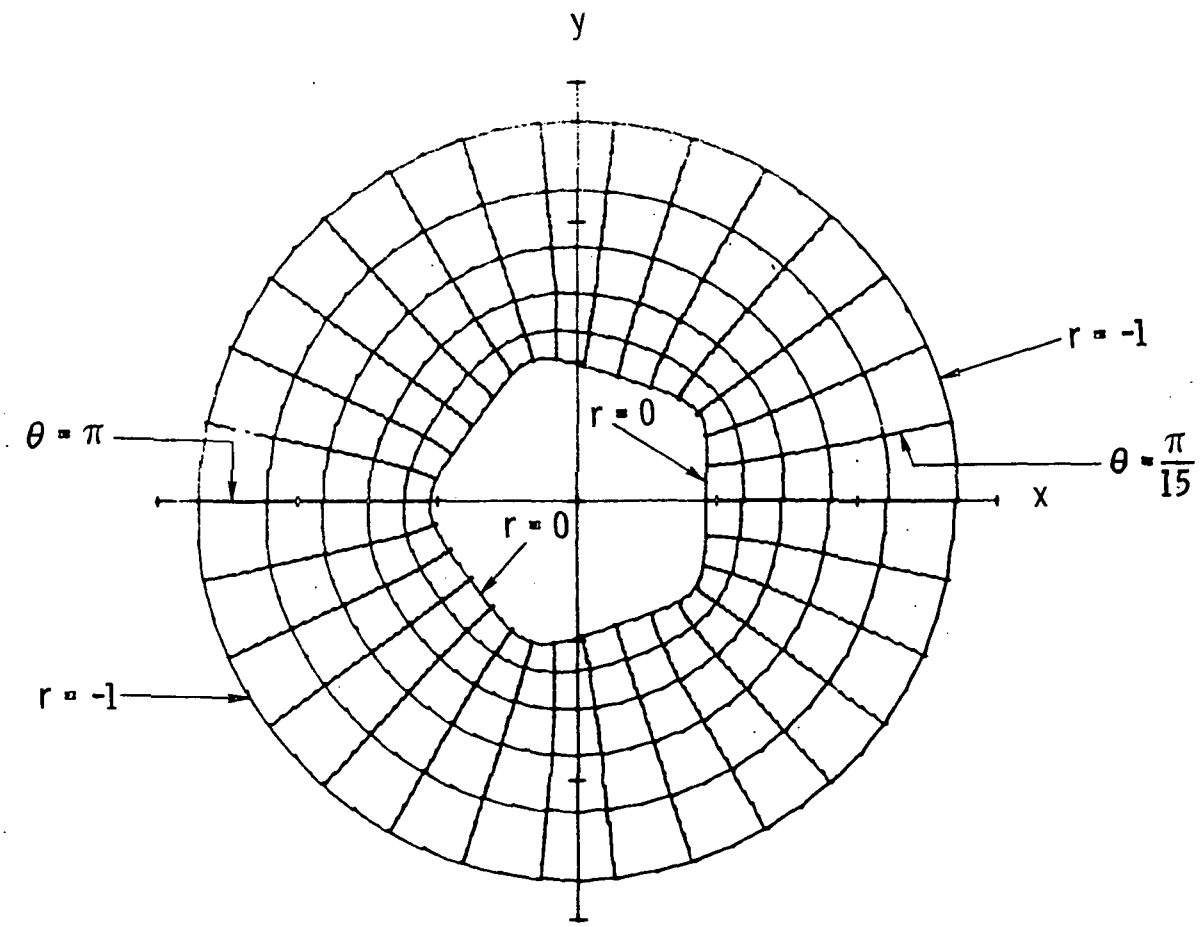

Figure 11.- Family of pentagonal shapes for N = 4.

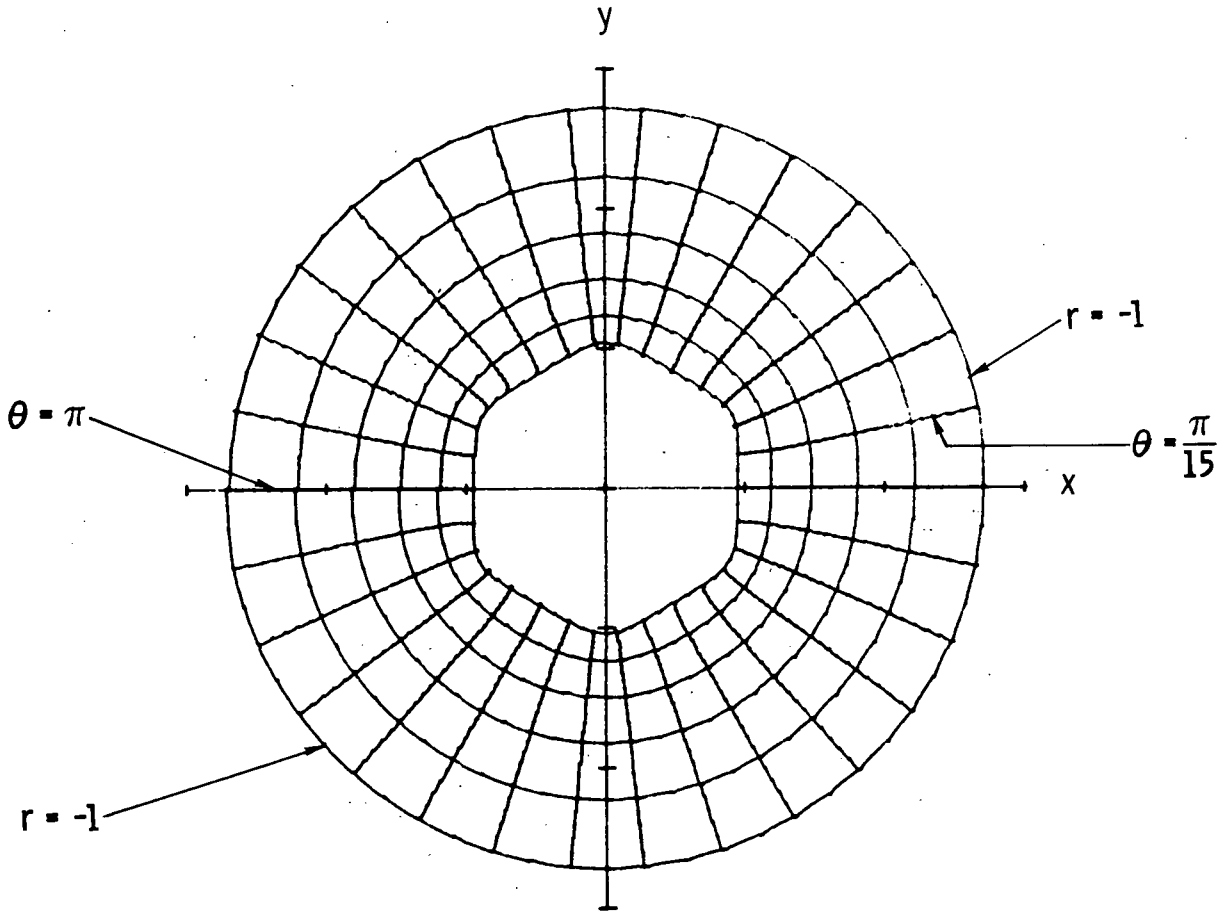

Figure 12.- Family of hexagonal shapes for N = 5.

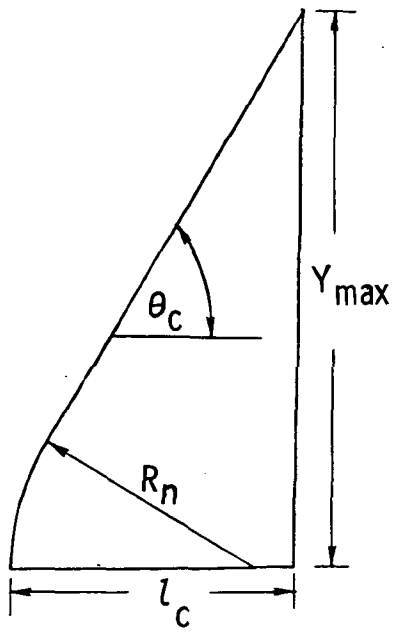

Figure 13.- Geometry of spherically capped cone.

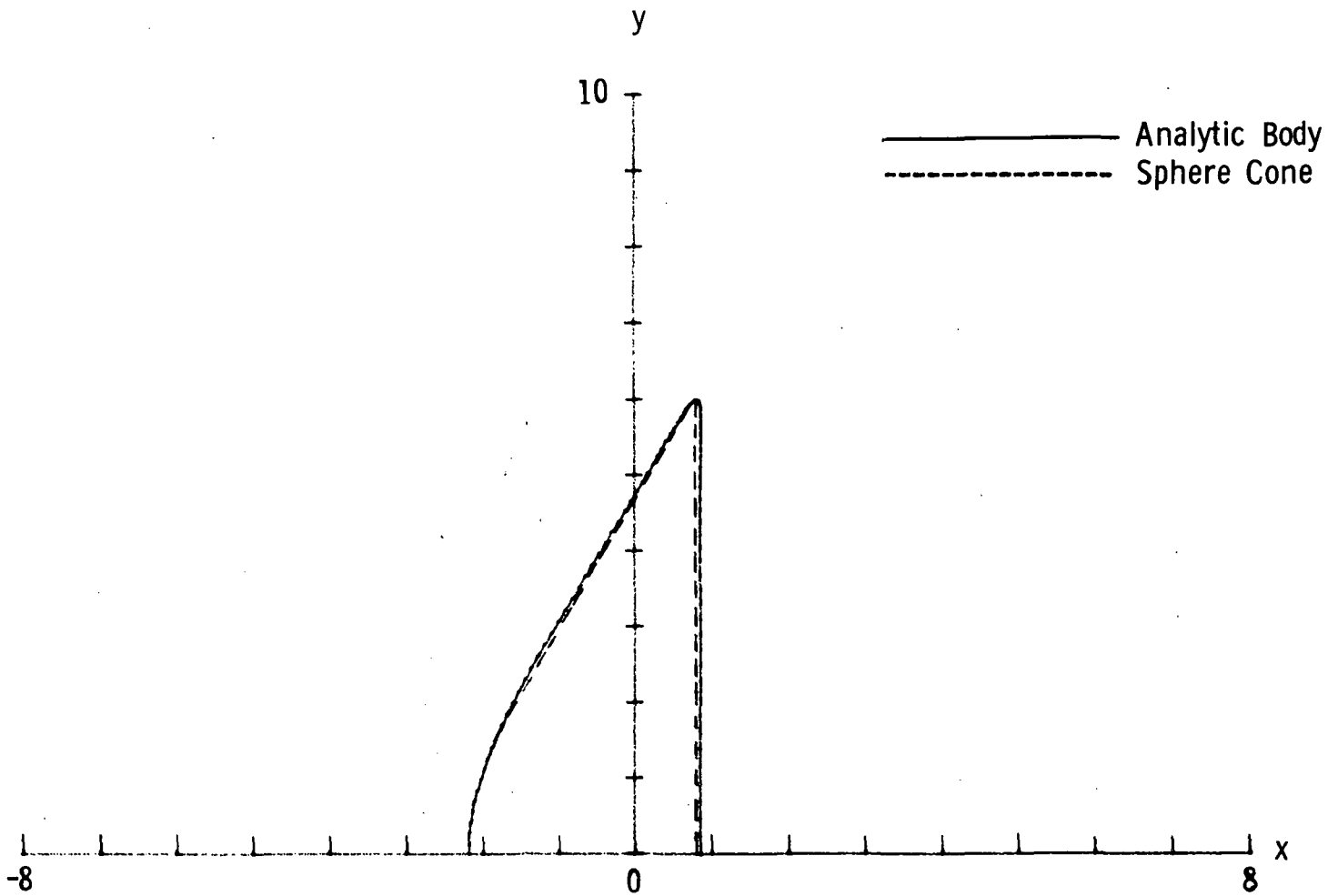

Figure 14.- 60^{o} sphere-cone approximation.

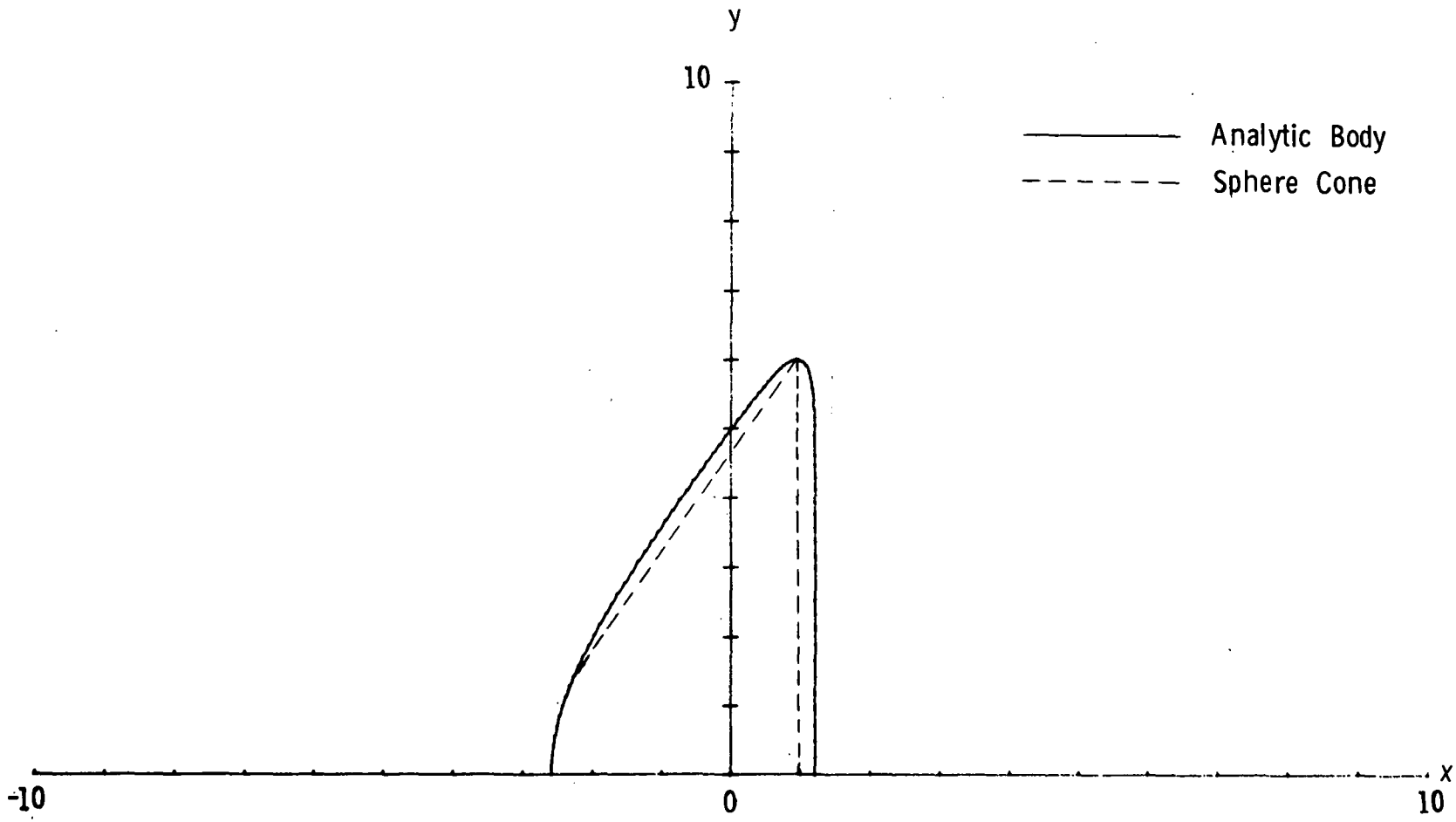

Figure 15.- 55^{o} sphere-cone approximation.

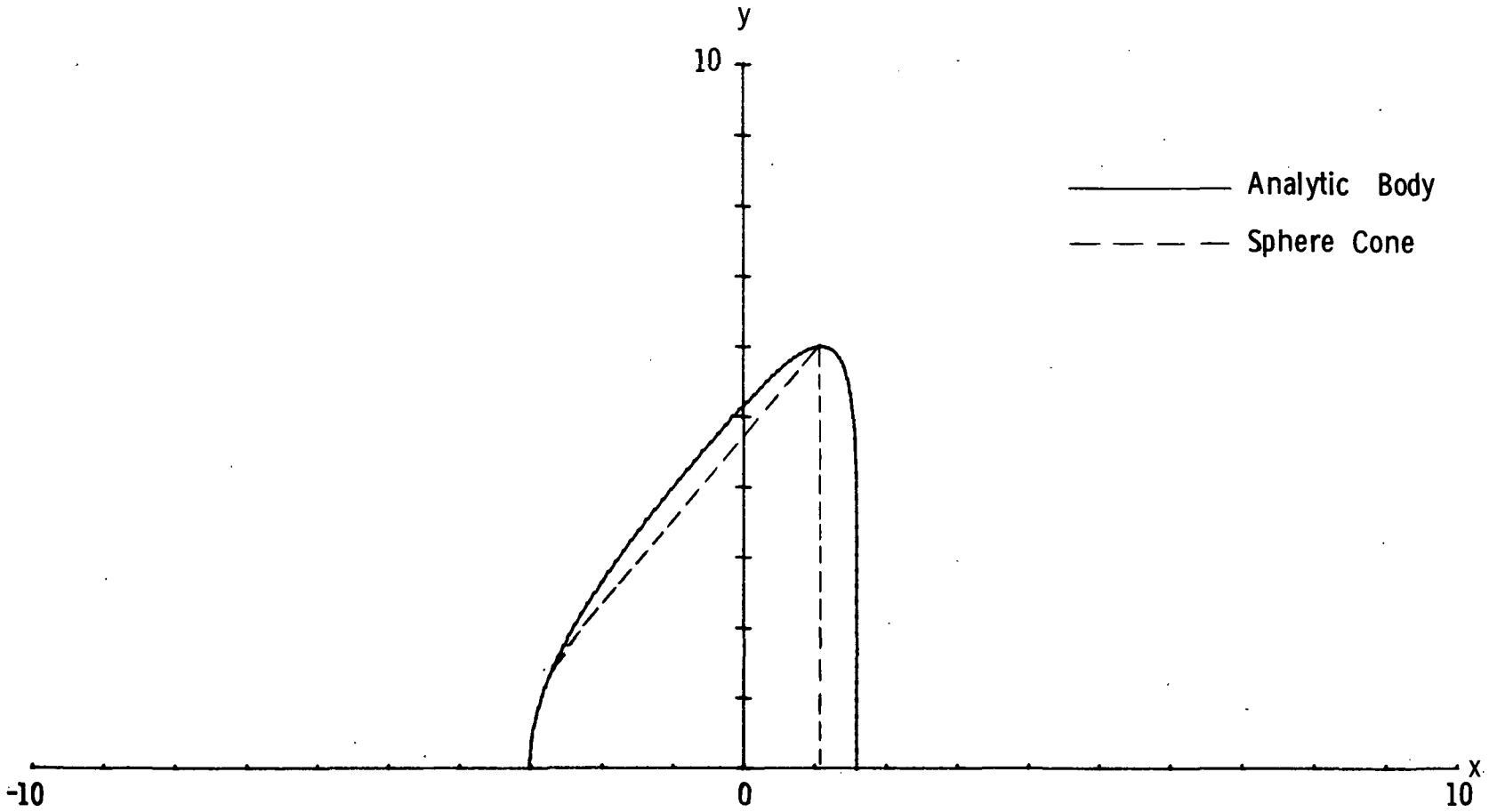

Figure 16.- 50^{O} sphere-cone approximation.

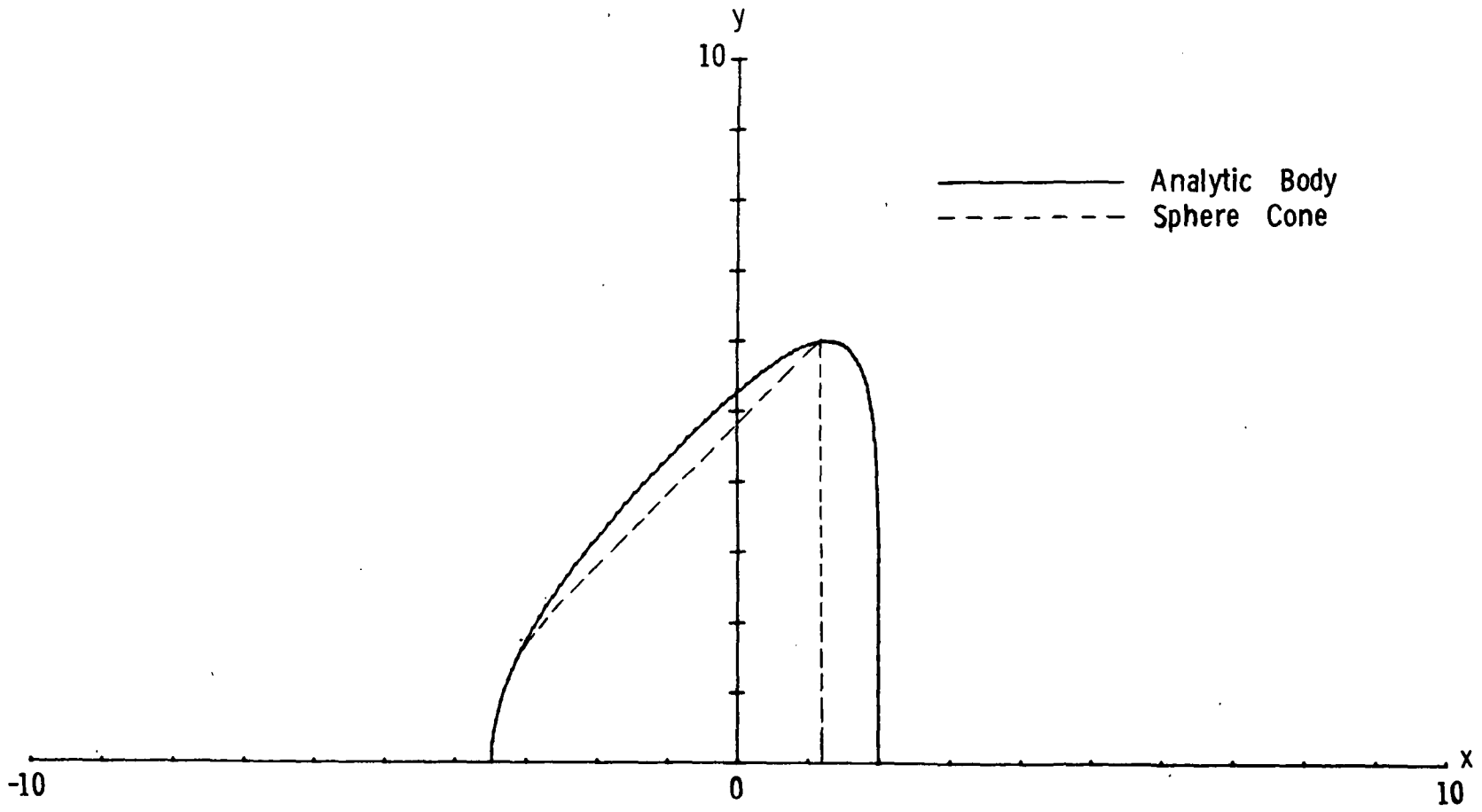

Figure 17.- 45° sphere-cone approximation.

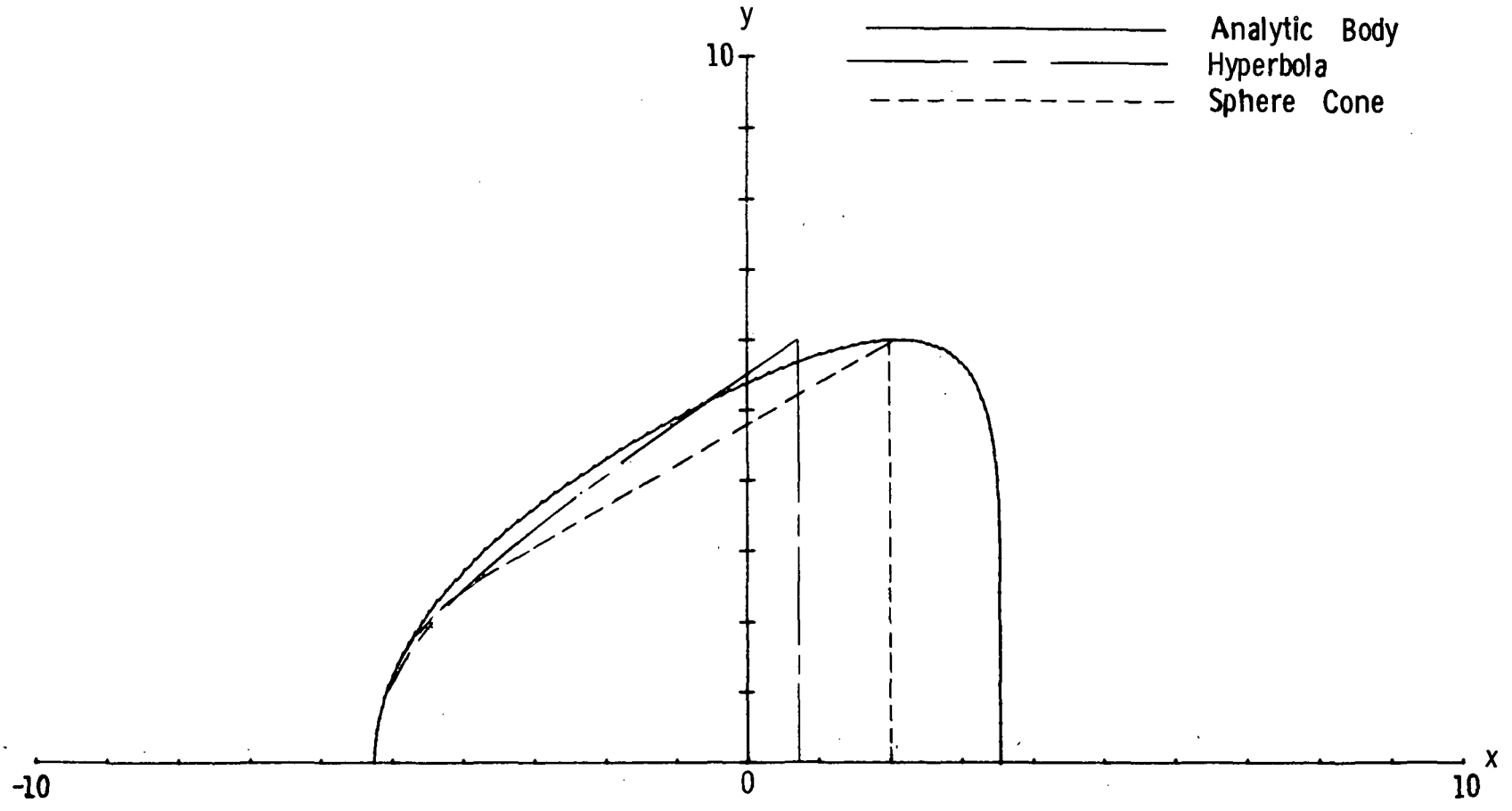

Figure 18.- 30° sphere-cone approximation.

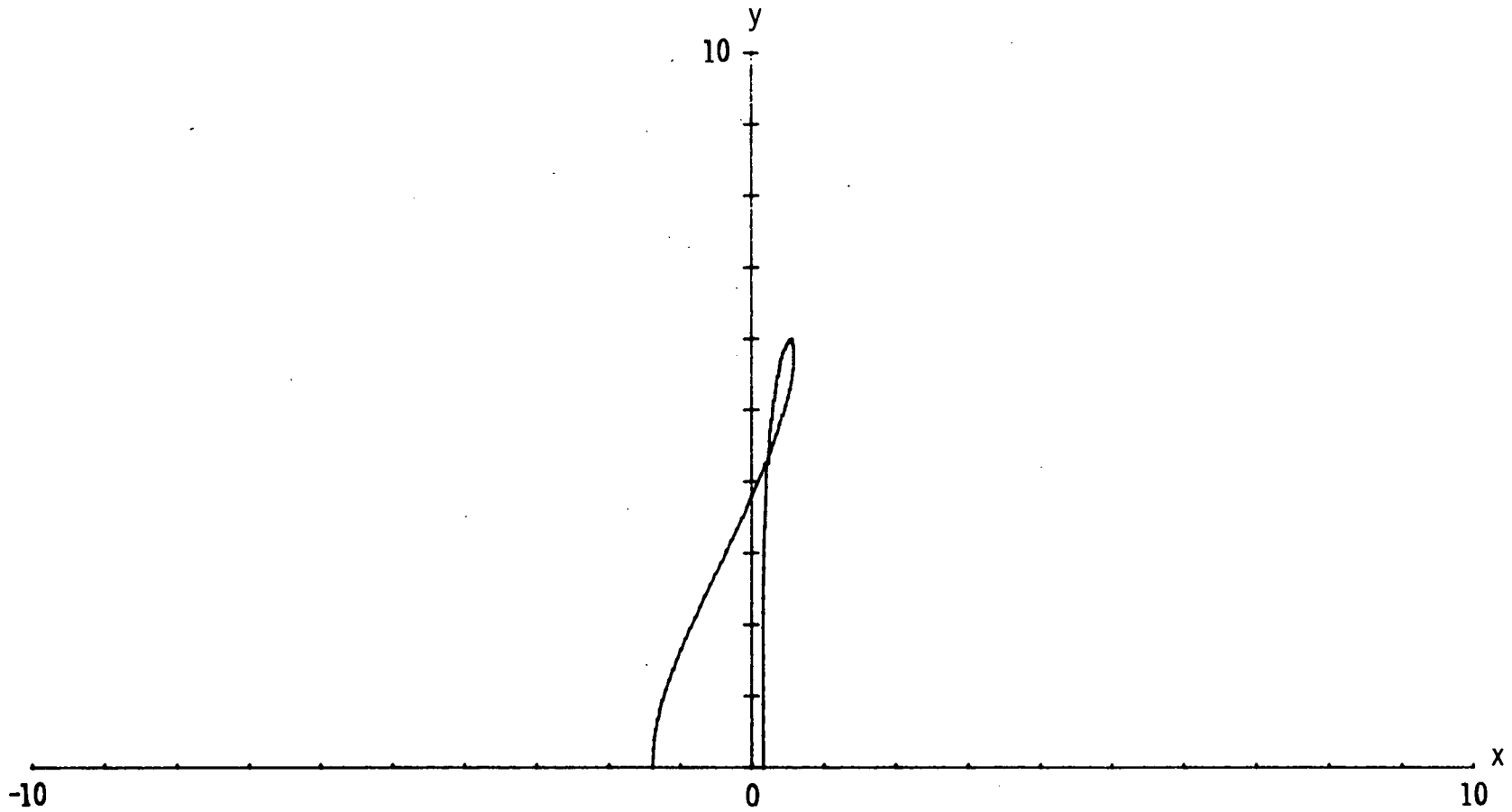

Figure 19.- 70^{o} sphere-cone approximation.

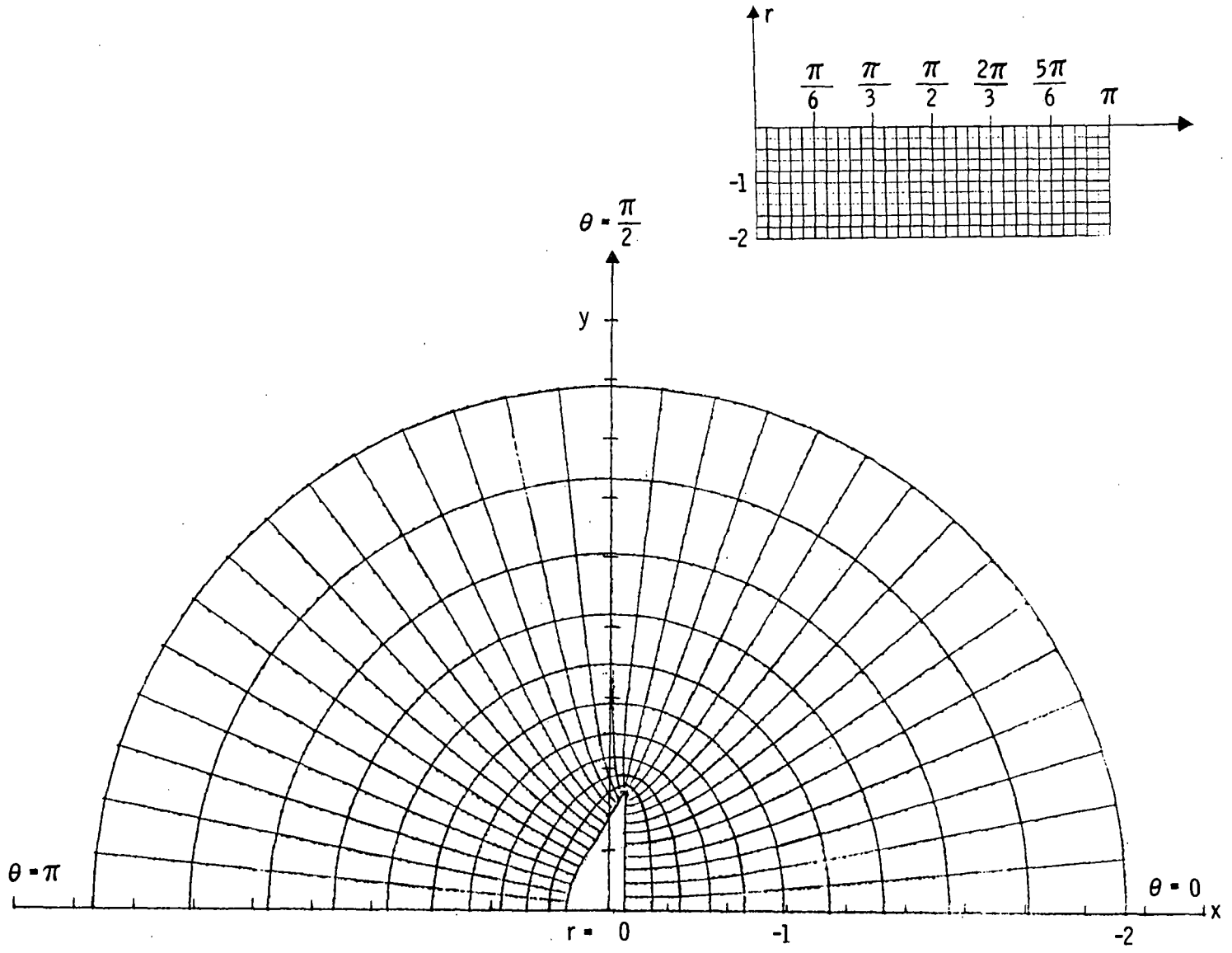

Figure 20.- Coordinate system around 60° sphere-cone approximation for $R_n = 1$ and $Y_{max} = 2$.

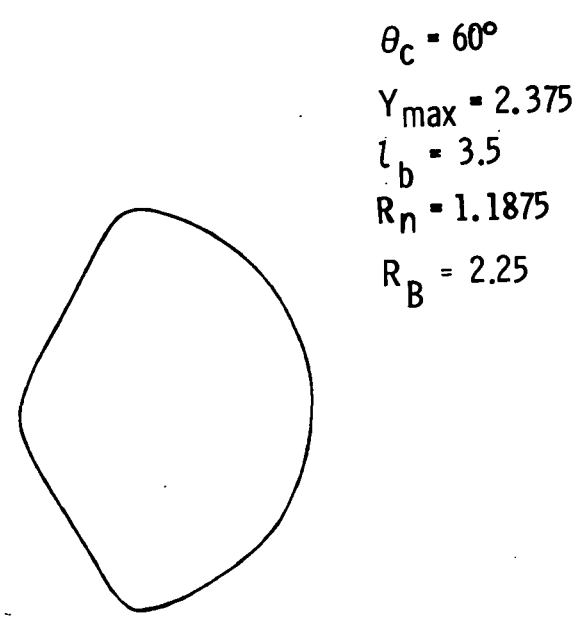

Figure 21.- Planetary probe vehicle.

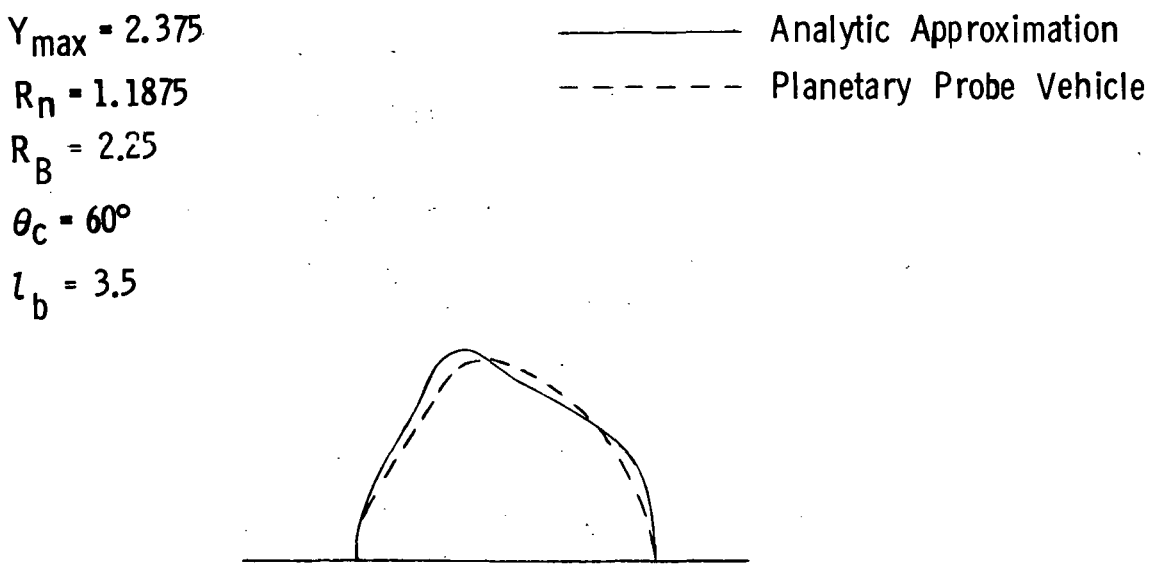

Figure 22.- Planetary probe-vehicle approximation.

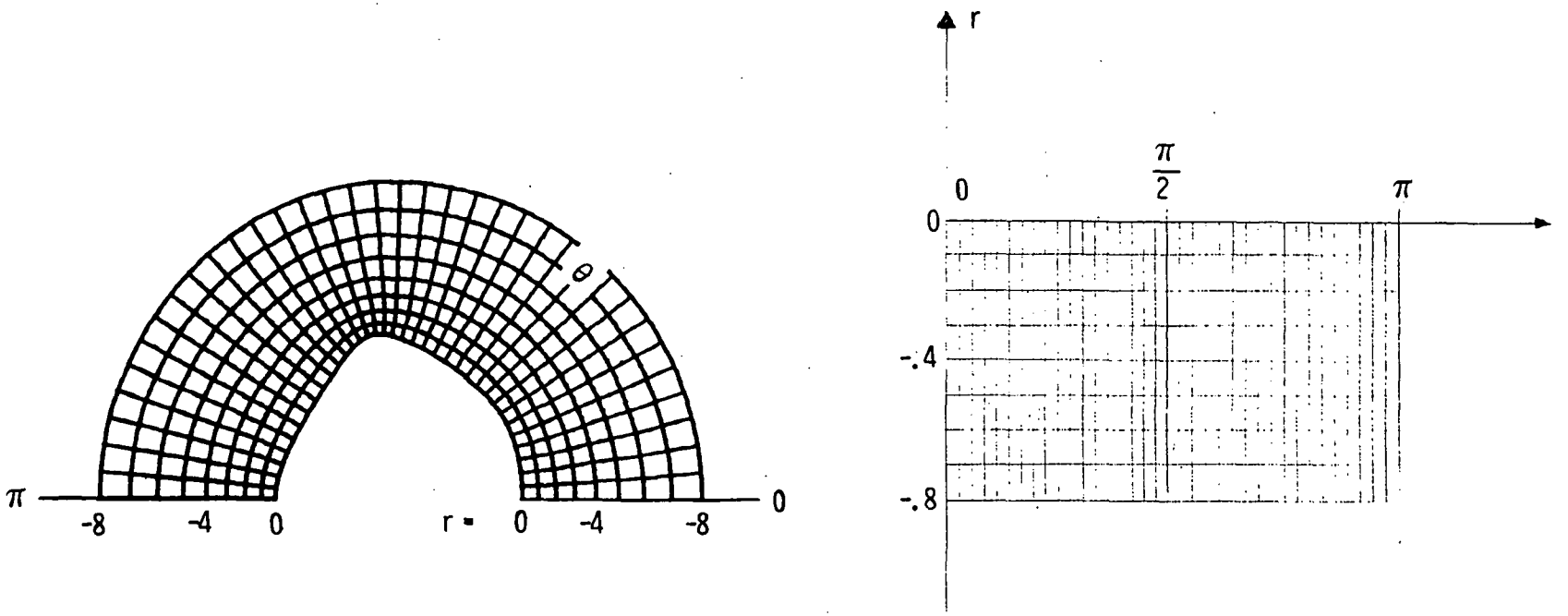

Figure 23.- Planetary probe-vehicle approximation with transformed coordinate system.

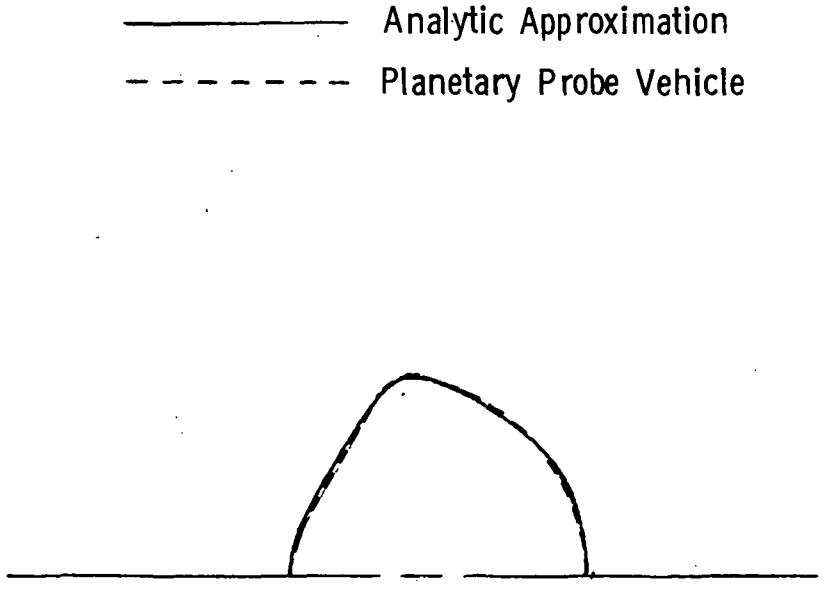

Figure 24.- Adjusted planetary probe-vehicle approximation.

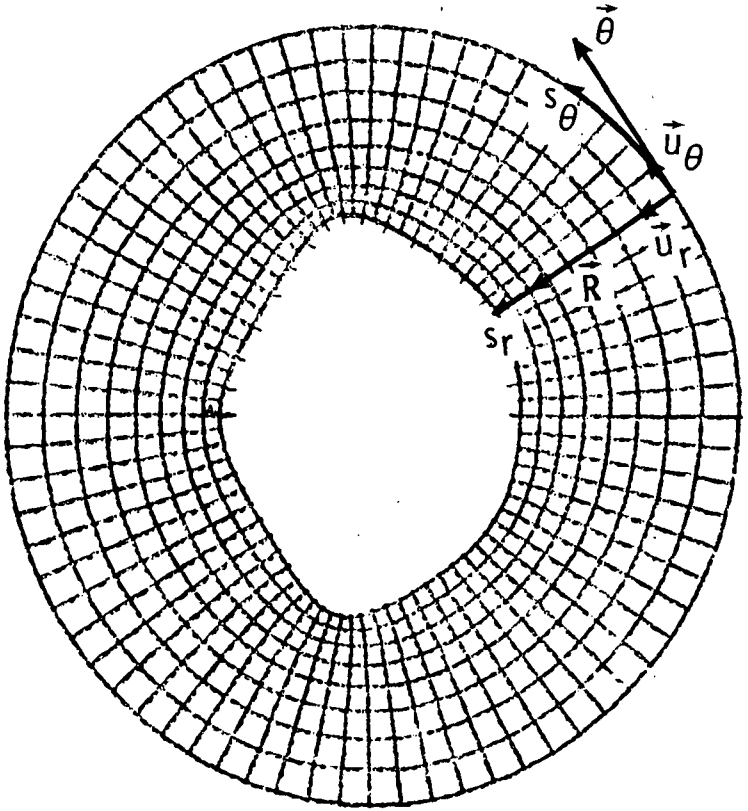

$\vec{\theta} = h_\theta \vec{u}_\theta$

$\vec{R} = h_r \vec{u}_r$

s_θ - Arc length increases in counter clockwise direction

s_r - Arc length increases toward body

Figure 25.- Schematic of vectors which determine metric coefficients.

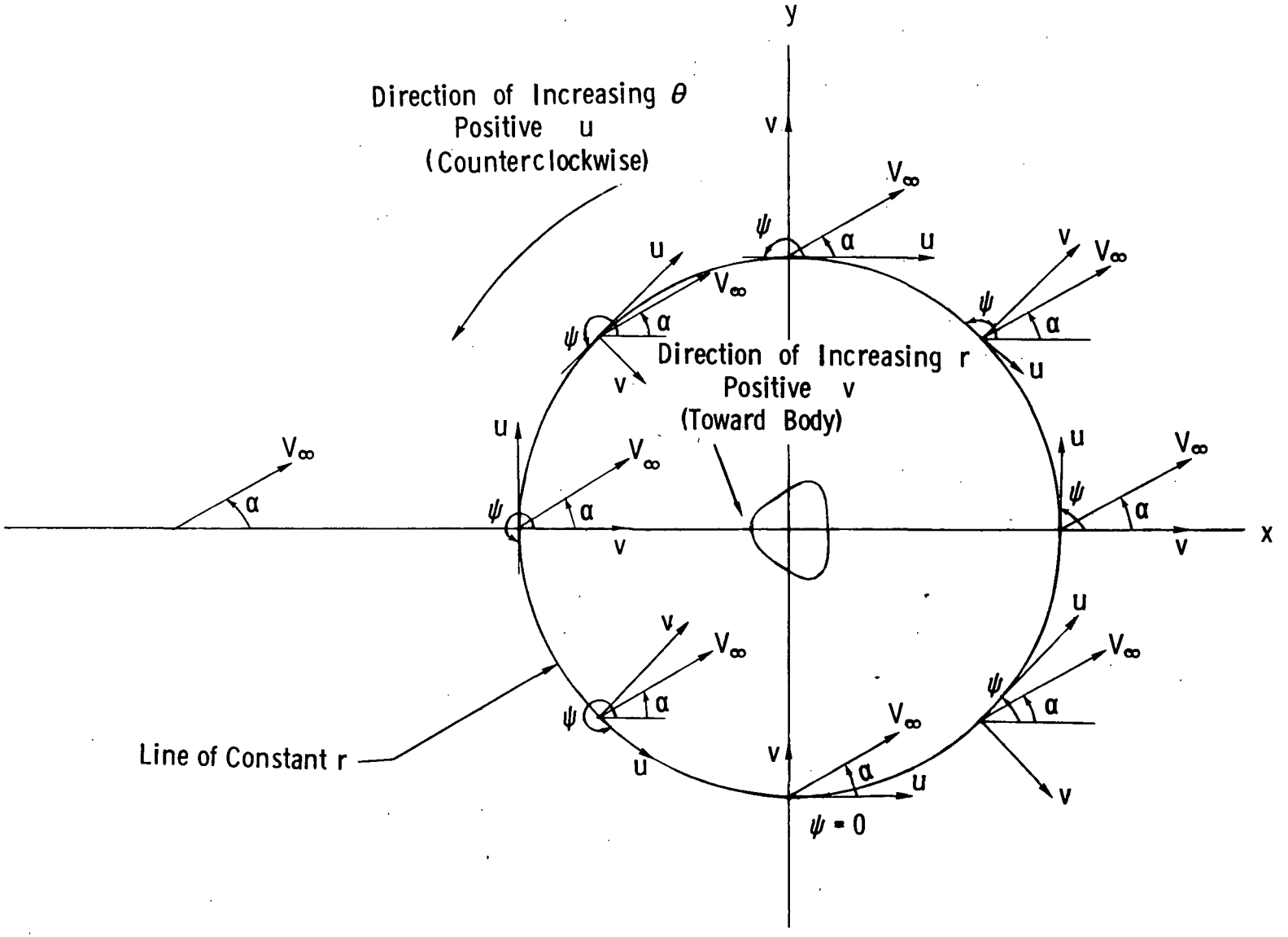

Figure 26.- Free-stream velocity components along line of constant r.

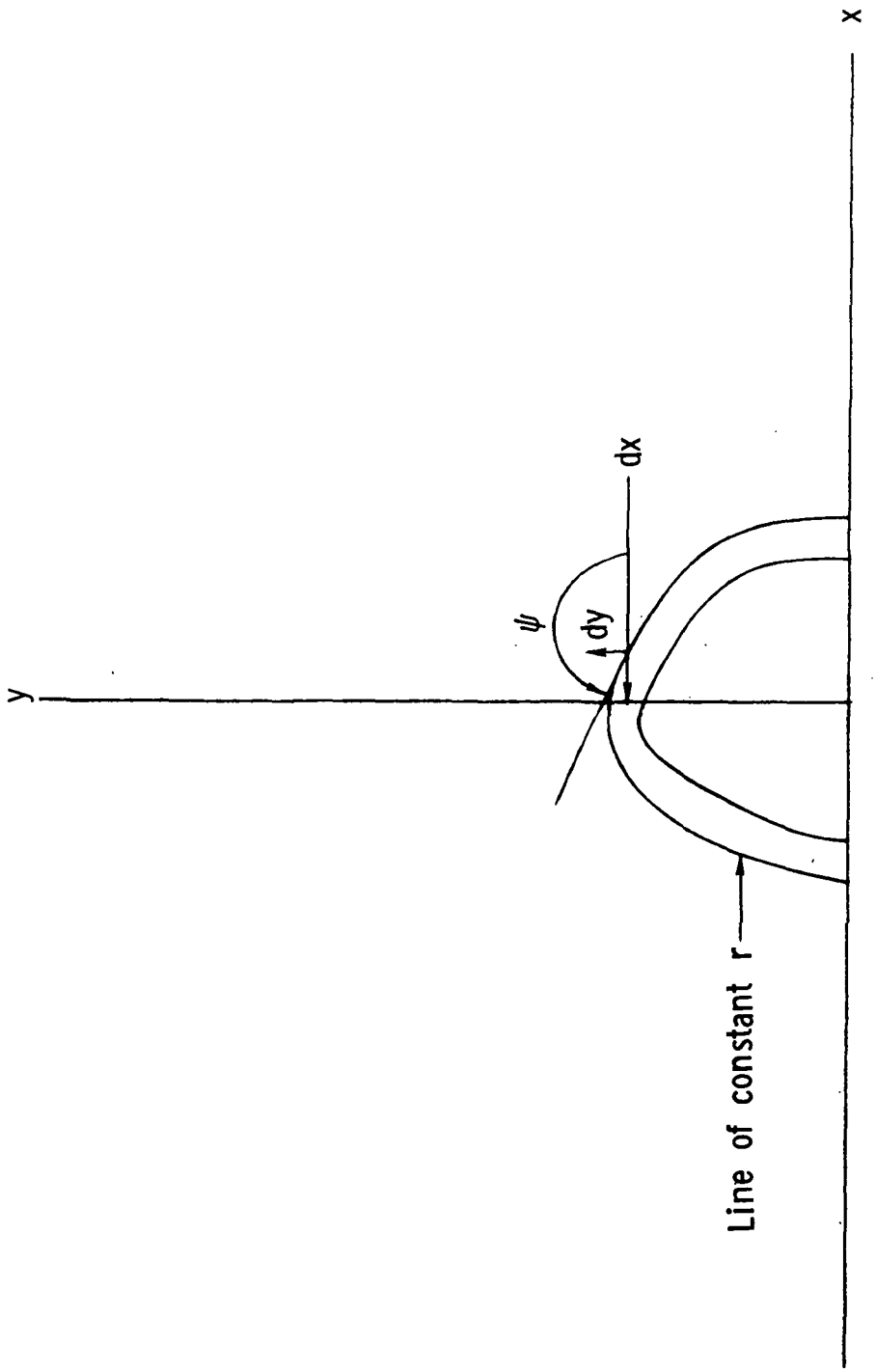

Figure 27.- Differentials along line of constant r.

"The aeronautical and space activities of the United States shall be conducted so as to contribute . . . to the expansion of human knowledge of phenomena in the atmosphere and space. The Administration shall provide for the widest practicable and appropriate dissemination of information concerning its activities and the results thereof."

—NATIONAL AERONAUTICS AND SPACE ACT OF 1958

NASA SCIENTIFIC AND TECHNICAL PUBLICATIONS

TECHNICAL REPORTS: Scientific and technical information considered important, complete, and a lasting contribution to existing knowledge.

TECHNICAL NOTES: Information less broad in scope but nevertheless of importance as a contribution to existing knowledge.

TECHNICAL MEMORANDUMS: Information receiving limited distribution because of preliminary data, security classification, or other reasons. Also includes conference proceedings with either limited or unlimited distribution.

CONTRACTOR REPORTS: Scientific and technical information generated under a NASA contract or grant and considered an important contribution to existing knowledge.

TECHNICAL TRANSLATIONS: Information published in a foreign language considered to merit NASA distribution in English.

SPECIAL PUBLICATIONS: Information derived from or of value to NASA activities. Publications include final reports of major projects, monographs, data compilations, handbooks, sourcebooks, and special bibliographies.

TECHNOLOGY UTILIZATION PUBLICATIONS: Information on technology used by NASA that may be of particular interest in commercial and other non-aerospace applications. Publications include Tech Briefs, Technology Utilization Reports and Technology Surveys.

Details on the availability of these publications may be obtained from:

SCIENTIFIC AND TECHNICAL INFORMATION OFFICE

NATIONAL AERONAUTICS AND SPACE ADMINISTRATION

Washington, D.C. 20546